NASA CR-127491

ANALYSIS OF VORTEX WAKE ENCOUNTER UPSETS

Walter A. Johnson and Gary L. Teper

SYSTEMS TECHNOLOGY, INC.
Hawthorne, Calif. 90250

August 1974

Prepared for

NATIONAL AERONAUTICS AND SPACE ADMINISTRATION
Washington, D. C. 20546

1. Report No.	2. Government Accession No.	3. Recipient's Catalog No.
NASA CR-127491		

4. Title and Subtitle	5. Report Date
ANALYSIS OF VORTEX WAKE ENCOUNTER UPSETS	August 1974
	6. Performing Organization Code

7. Author(s)	8. Performing Organization Report No.
Walter A. Johnson and Gary L. Teper	TR-1025-2

9. Performing Organization Name and Address	10. Work Unit No.
Systems Technology, Inc. 13766 South Hawthorne Boulevard Hawthorne, California 90250	11. Contract or Grant No. NAS4-1952
	13. Type of Report and Period Covered Contractor Report - Final
12. Sponsoring Agency Name and Address National Aeronautics and Space Administration Washington, D. C. 20546	14. Sponsoring Agency Code

15. Supplementary Notes

Project Manager, Herman A. Rediess, Vehicle Dynamics and Control Division, NASA Flight Research Center, Edwards, Calif

16. Abstract

The problem of an airplane being upset by encountering the vortex wake of a large transport on takeoff or landing is currently receiving considerable attention. This report describes the technique and results of a study to assess the effectiveness of automatic control systems in alleviating vortex wake upsets. A six-degree-of-freedom nonlinear digital simulation was used for this purpose. The analysis included establishing the disturbance input due to penetrating a vortex wake from an arbitrary position and angle. Simulations were computed for both a general aviation airplane and a commercial jet transport. Dynamic responses were obtained for the penetrating aircraft with no augmentation, and with various command augmentation systems, as well as with human pilot control. The results of this preliminary study indicate that attitude command augmentation systems can provide significant alleviation of vortex wake upsets; and can do it better than a human pilot.

17. Key Words	18. Distribution Statement
Vortex encounter simulation Vortex upset alleviation Automatic control systems	Unclassified - Unlimited

19. Security Classif. (of this report)	20. Security Classif. (of this page)	21. No. of Pages	22. Price*
Unclassified	Unclassified	88	$3.75

*For sale by the National Technical Information Service, Springfield, Virginia 22151

TABLE OF CONTENTS

LIST OF FIGURES

SECTION I

INTRODUCTION

Several incidences have occurred in which an airplane has been severely upset by flying into the vortex wake of a large jet transport during landing approach or takeoff. A number of these encounters involving general aviation type aircraft and one involving a jet transport resulted in fatal crashes (Ref. 7). Flight tests reported in Ref. 8 further confirm the inability of a pilot to cope with the severe upsets. To reduce such severity, considerable effort is being spent to predict the wake locations, and to find ways of dissipating the vortices without degrading the performance of the generating aircraft. An alternate approach is to attempt to reduce the response of the penetrating aircraft to an acceptable level by means of an automatic control system.

A brief study was conducted to determine the potential usefulness of command augmentation systems for alleviating vortex wake encounter upsets and to identify those characteristics of the automatic systems that are desirable and those that are undesirable. It is emphasized that the study was preliminary and only meant to give a first-order assessment of the feasibility of the approach.

A six-degree-of-freedom, nonlinear digital simulation was used to analyze the dynamic response of an aircraft as it traverses a vortex wake. The study consisted of: establishing the disturbance input due to penetrating a vortex wake; developing a dynamic simulation of an aircraft penetrating a vortex wake from an arbitrary position and angle; computing the responses of two types of aircraft, with and without automatic control systems, when penetrating the vortex wake from the most critical angles; and assessing the effectiveness of several types of automatic control systems to alleviate vortex wake encounter upsets.

The two example aircraft simulated were a general aviation airplane penetrating the vortex wake of an executive jet transport at separations of 3 and 10 miles, and the wake of a commercial jet transport at 3 miles separation; and a commercial jet transport penetrating the vortex wake of a jumbo jet transport at a separation of 3 miles. The types of automatic

control systems considered were bank angle command, heading command, and roll rate command. In each case a pitch command system was also used. The simulation included pilot control inputs as well as control system inputs.

This report describes the simulation used and the results obtained. Previous studies have considered the effects of a vortex wake on a trailing aircraft. Reference 1 calculated the static moments produced assuming the aircraft was placed at the worst location in the vortex. Complete digital simulations of the dynamic response of an aircraft penetrating a vortex wake were used in Refs. 7 and 13; however, they did not assess automatic control systems for possibly alleviating the upset, the primary thrust of this report.

The succeeding sections of this report are organized as follows. Section II defines the vortex model used and describes the resulting flow patterns. Section III describes the strip theory aerodynamics used in the simulation. Section IV summarizes the digital computer simulation features. Section V defines the penetrating aircraft and test conditions considered. Section VI describes the control systems and human pilot model used. Section VII includes typical time traces of vortex encounter upsets and a discussion of their significance. Section VIII presents an analysis of the sensitivity of vortex upsets to vortex model parameters. Section IX summarizes the results and conclusions of the study. And, finally, several appendices are used to present detailed information in support of the material included in the body of this report. This information is included in appendices so the reader is not sidetracked by lengthy derivations, etc. that would otherwise be in the main text.

SECTION II

VORTEX MODEL AND FLOW DESCRIPTION

As might be expected, most of the mathematical models for vortex tangential velocity give qualitatively similar flow patterns. That is, zero flow at the center of the vortex core; flow building up to a maximum at some "core radius;" and then a falling off of flow magnitude for radial distances larger than the "core radius". But the detailed fitting of measured vortex flow data with any of the theoretically derived analytical expressions has met with varying degrees of success in the past (e.g., Refs. 1-3). Therefore, it was not immediately obvious which model to use in our simulation. However, after consideration of the alternatives, it was deemed adequate for our purposes to use the following vortex model, taken from Ref. 1. (This is often referred to as the "Lamb" model.) The model is defined by the tangential flow characteristics given in Eq. II-1. (Axial flow was ignored, thus giving a two-dimensional flow. The reason for not including axial flow is that no good model for it is known.)

$$V_\theta = \frac{\Gamma_o}{2\pi r}\left[1 - e^{-(r^2/4\epsilon\tau)}\right] \qquad \text{(II-1)}$$

where

V_θ is the tangential vortex velocity

$\Gamma_o = 4W_G/\pi\rho V_G b_G$ is the total circulation, which represents the strength of the vortex (it is a function of the weight, speed, and wing span of the generating airplane)

$\epsilon = 0.0002\ \Gamma_o$ represents the vortex decay effect

τ represents the age of the vortex

r is the radial distance from the center of the vortex

Equation II-1 can be manipulated to give the following useful relations (see Appendix A for derivation):

$$\Gamma_o = 4.40\, d_{CORE} V_{\theta_{max}} \qquad \text{(II-2)}$$

$$4\epsilon\tau = .20\, d^2_{CORE} \qquad \text{(II-3)}$$

The centers of the two vortices behind the generating airplane are assumed to be straight lines at a constant altitude, parallel to each other at a distance $(\pi/4)b_G$ apart (Ref. 1). A sketch of the resulting vertical flow from both vortices is shown along with the generating airplane in Fig. II-1, while Fig. II-2 shows an actual plot of the computed vertical flow 3 miles behind the Jetstar, along with a scaled overlay of the PA-30 for reference.

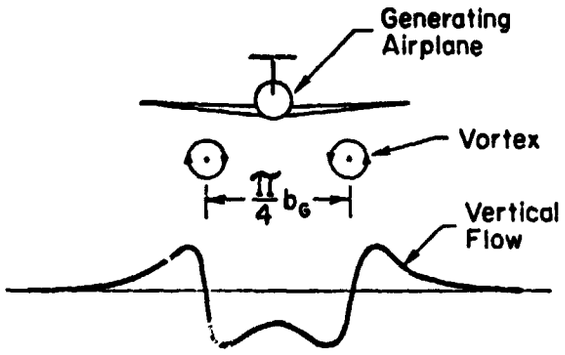

Figure II-1. Sketch of the Vortex Flow Field

Table II-1 presents some pertinent numerical values for a single vortex from several generating airplanes. The numbers shown for the C-5A and the Jetstar were computed using airplane weight and geometry in Eq. II-1, while the numbers for the B-727 were obtained by fitting a curve of the form of Eq. II-1 to tower data taken at NAFEC (Ref. 4), and then using Eq. II-2 to compute the core diameter. The specific technique for using measured data to compute the vortex parameters is as follows (see Appendix A):

- Determine Γ_o from the flow well outside the core ($V_\theta \doteq (\Gamma_o/2\pi r)$ for $r > 2r_{CORE}$)
- Use $V_{\theta_{max}}$ (from data) along with Γ_o to determine d_{CORE} (via Eq. II-2)

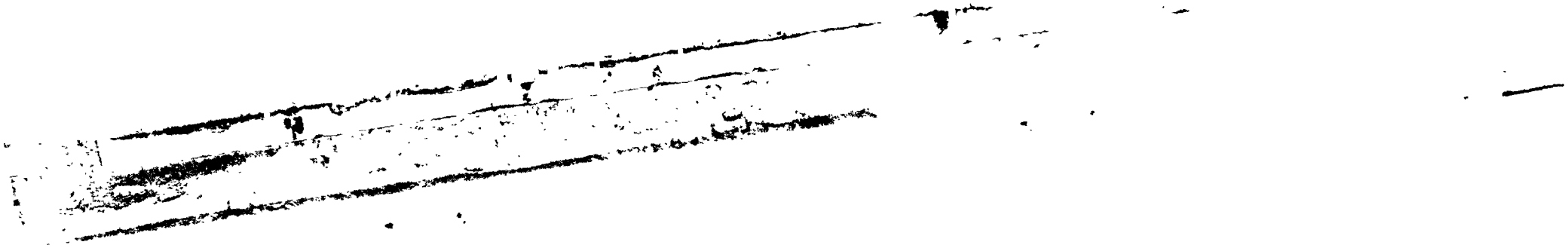

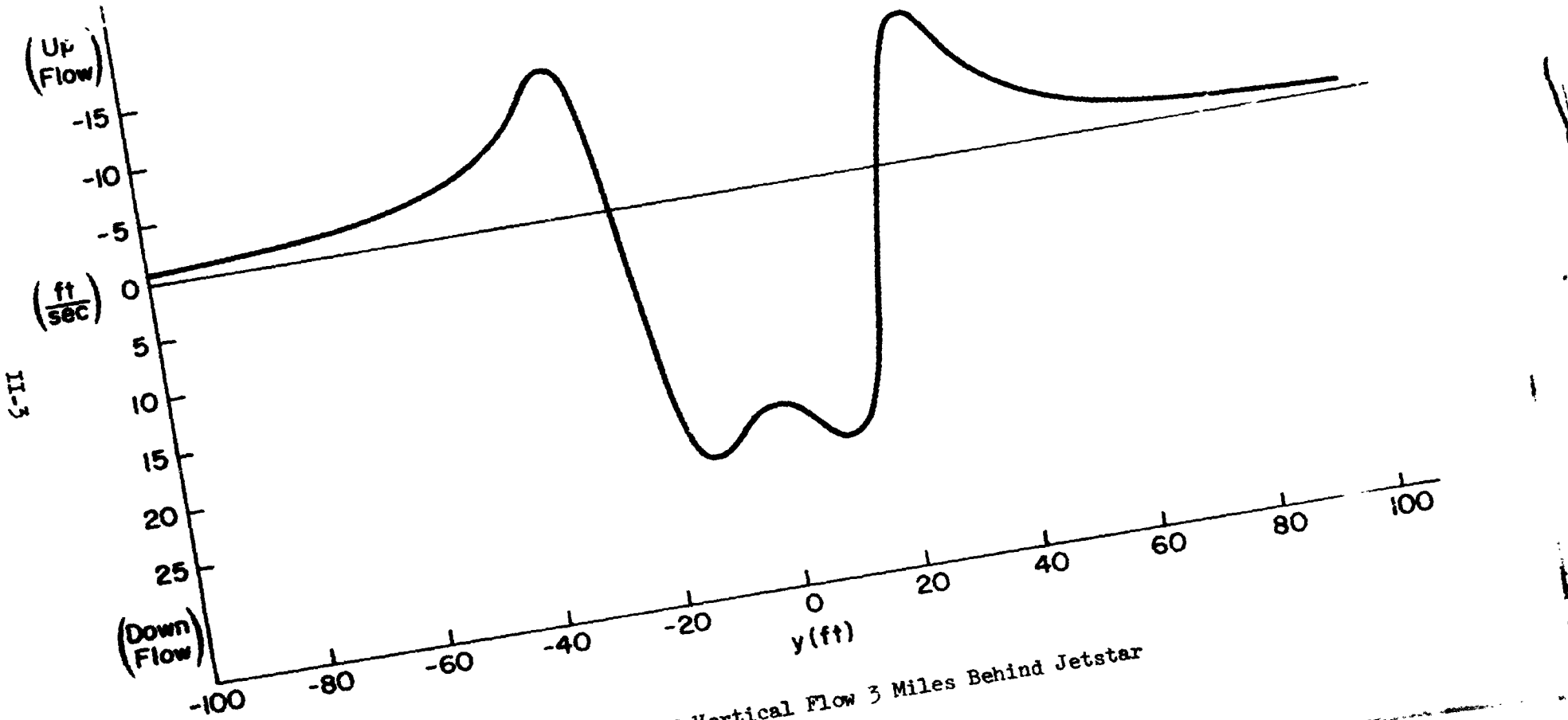

Figure II-2. Computed Vertical Flow 3 Miles Behind Jetstar

TABLE II-1. TANGENTIAL FLOW CHARACTERISTICS OF A SINGLE VORTEX

GENERATING AIRPLANE	SEPARATION DISTANCE	RADIUS FOR MAXIMUM VELOCITY	MAXIMUM VELOCITY	TOTAL CIRCULATION*
C-5A	3 mi	19.5 ft	34 ft/sec	5834 ft^2/sec
Jetstar	3 mi	8.5 ft	17 ft/sec	1272 ft^2/sec
	10 mi	15.6 ft	9 ft/sec	1236 ft^2/sec
B-727	1.5 mi	.85 ft	209 ft/sec	1563 ft^2/sec

*It is noted that the value of circulation computed using the Lamb model does not always agree with the circulation that would be measured. This is due to the fact that the falloff of vortex tangential velocity with radial distance is, in reality, a function of the spanwise distribution of lift on the wing which generated the vortex. Because the Lamb model assumes a 1/r falloff, values of circulation computed via the Lamb model may not be accurate. However, for our present purposes we are not really concerned with the numerical value of circulation, nor with the exact falloff of flow with radius. Therefore, this inadequacy of the Lamb model is not significant here.

SECTION III

STRIP THEORY CONSIDERATIONS

A. STRIP THEORY GEOMETRY

Because the encountered vortices can produce a highly nonuniform local flow over the lifting surfaces of the penetrating airplane, strip theory was used to compute the forces and moments caused by the vortex flow (see Ref. 5). To implement this, the penetrating airplane was assumed to have three lifting surfaces: a wing, a horizontal tail, and a vertical tail. Each of these surfaces was divided into chord-wise strips as shown in Fig. III-1. The wing was divided into 20 strips per semi-span, while the horizontal and vertical tails were each divided into 6 strips per semi-span. Stall was accounted for by limiting the maximum (and minimum) lift coefficient on each strip. The distributed forces along the fuselage were modeled via a pitching moment and a yawing moment respectively proportional to the vortex-flow-induced incremental angles of attack and sideslip measured at the wing 1/4 root chord.

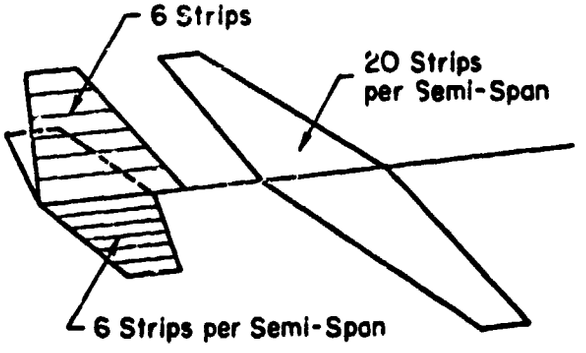

Figure III-1. Strip Theory Geometry

No lift-lag function was used because our primary attention was confined to the near axial encounters where non-stationary effects would be expected to be minimal.

B. FLOW AT EACH STRIP

The flow at each strip (due to the vortex pair from a generating airplane) was determined by superimposing the flow from each of the two vortices as indicated in Fig. III-2. A detailed derivation of the pertinent equations for the flow at each strip is included in Appendix B.

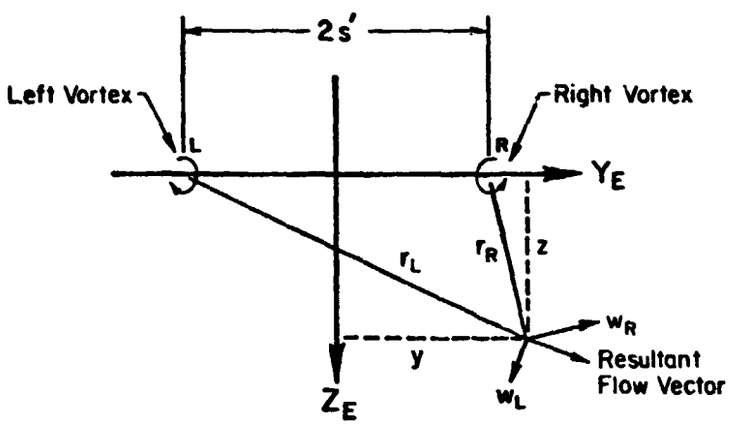

Figure III-2. Flow at an Arbitrary Point in Space (y, z) Due to the Left and Right Vortices of a Generating Airplane (w_L and w_R are the tangential flow magnitudes of the left and right vortices, respectively.)

C. MATCHING STRIP THEORY TO KNOWN VEHICLE CHARACTERISTICS

At each instant in time the total forces and moments on the penetrating airplane are obtained by adding the forces and moments due to the vortex flow alone to the forces and moments that would exist in the absence of the vortex flow (for the instantaneous values of airplane attitude and motion). However, the forces and moments due to the vortex flow are computed via strip theory, while those due to airplane attitude and motion are computed via non-dimensional aerodynamic derivatives. To obtain a correct set of total forces and moments, it is necessary that the strip theory description of the airplane gives the same aerodynamic characteristics as obtained via the non-dimensional derivatives. To insure the

achievement of this compatibility, the magnitudes of several of the strip theory parameters are adjusted slightly. Table III-1 lists the four dimensional stability derivatives (representing the key aerodynamic properties) that were selected for matching, as well as the strip theory parameters that can be adjusted to effect the matching.

TABLE III-1

PARAMETERS USED FOR MATCHING STRIP THEORY CALCULATIONS TO KNOWN VEHICLE AERODYNAMIC CHARACTERISTICS

KNOWN VEHICLE CHARACTERISTICS	STRIP THEORY PARAMETERS TO BE ADJUSTED
Z_w	$C_{L_{\alpha_W}}$
M_w	$C_{L_{\alpha_H}}$, $\frac{d\epsilon}{d\alpha}$, M_{α_F}
N_β	$C_{L_{\alpha_V}}$, $\frac{d\sigma}{d\beta}$, N_{β_F}
L_p	$C_{L_{\alpha_W}}$ as f(y)

where

W ≡ Wing
H ≡ Horizontal tail
V ≡ Vertical tail
F ≡ Fuselage

SECTION IV

COMPUTER SIMULATION FEATURES

A. COMPUTATION LOGIC

The basic logic for computing the dynamic effects of a vortex encounter are listed below.

(1) Start with known aircraft c.g. location and attitude.

(2) Select strip to be considered.

(3) Define location of point on desired strip in body-fixed axis system.

(4) Transform location of desired point to earth-fixed axis system.

(5) Compute 2-dimensional earth-referenced flow at point of interest in space due to both vortices.

(6) Transform earth-referenced flow at point of interest to body axis system in aircraft.

(7) Compute $\Delta\alpha$ (or $\Delta\beta$, as appropriate) on desired strip.

(8) Compute ΔForce on strip (due to vortex flow).

(9) Repeat (2) through (8) for each strip.

(10) Sum the forces and forces × lever arms for each strip to get forces and moments on aircraft due to vortex flow.

(11) Add forces and moments due to vortices to forces and moments due to aircraft attitude and velocity (obtained via non-dimensional stability derivatives), giving total forces and moments on aircraft.

(12) Integrate aircraft equations of motion over small Δt to obtain new c.g. location and attitude.

(13) Repeat (1) through (12) until desired time of flight is reached.

(14) Store results and then plot.

B. SIMULATION FEATURES

The salient features of the computer simulation are listed in Table IV-1.

TABLE IV-1

SALIENT FEATURES OF THE COMPUTER SIMULATION

- 6-degree-of-freedom nonlinear digital simulation
- Arbitrary generating and penetrating airplanes
- Arbitrary initial conditions (penetration angles and position)
- Can use any vortex model desired
- No small-angle approximations for Euler angles
- Includes control surface position and rate limits
- Arbitrary control system logic
- Subroutine calculations:
  1) Vortex flow at any point
  2) Transform flow into body axes
  3) Compute force on each strip via strip theory
  4) Sum individual forces and forces × lever arms
  5) Numerical integration of equations of motion

C. "RAIL" ENTRY PROVISION

Provision was made in the computer program to constrain the penetrating airplane's c.g. to a straight line path (as if on a "rail") until an arbitrarily selectable "release range" from one of the vortices is reached—whereupon the airplane is totally released to perform whatever maneuvers the aerodynamic forces and moments (and gravity) produce. It is emphasized that only the three translational degrees of freedom are constrained prior to release. That is, the airplane is completely free to rotate about all three axes even prior to release of the c.g.

The purpose of this artificial constraint is twofold. First, it insures that the penetrating airplane will hit the vortex core; and, second, it provides a means for obtaining repeatability of entry conditions nece sary

for making comparisions of various airplane or control system configurations. The question of the validity of the subsequent upset naturally arises here. This was the first item to be checked when the rail entry was considered. It turns out that an encounter with the rail constraint is equivalent to a free flight encounter with different "initial" conditions far from the vortex, but with the same conditions as the vortex core is penetrated. There are small differences in some of the airplane variables, but these are very minor for our purposes, and certainly a small price to pay for the advantages gained.

SECTION V

AIRCRAFT AND TEST CONDITIONS

Example vortex wake encounters were simulated for two classes of aircraft: a 3,200 pound, twin-engine general aviation airplane (PA-30, "Twin Comanche") penetrating the vortex wakes of a 30,000 pound executive jet transport (Jetstar), and a 140,000 pound commercial jet transport (B-727); and a 126,000 pound commercial jet transport (CV-880) penetrating the vortex wake of a 580,000 pound jumbo jet transport (C-5A). For the PA-30, 3 and 10 mi separations were used, while for the CV-880 a 3 mi separation was simulated. The penetrating airplanes were in "final approach" configurations. These aircraft were selected because the aerodynamic data were readily available to the investigators.

Digital simulations were calculated for penetrations both perpendicular and parallel (approximately) to the vortex wake axes. For the perpendicular penetrations the primary measure of the severity of an encounter is peak normal load factor, while for glancing encounters the primary measure is the maximum bank angle during the upset.

Two types of glancing encounters were considered — a glancing entry into the side of one vortex (from "outside" the vortex pair), and a glancing entry into the bottom of one vortex. These differed in one significant aspect. The side entry first produced roll in one direction (as the vortex was approached), and then suddenly rolled the vehicle over in the opposite direction (as the center of the vortex as encountered). The entry from below produced roll in one direction only. For the particular control systems used, and the entry conditions tried, larger peak bank angles were obtained with the entries from below. Therefore, all of the various comparisons made were based on results for entries from below.

The simulated encounters, with and without the automatic control systems, for all of the CV-880 runs, and for the PA-30 runs with the Jetstar vortices were made with no human pilot control action. Thus, the

comparisons for these aircraft combinations are made between the situation in which no action is taken to arrest the upset and that in which the control system is operating to arrest the upset. A better comparison would include the action of the pilot-in-the-loop, but this was only done for the PA-30 encountering B-727 vortices.

SECTION VI

CONTROL SYSTEM MODELS

Several types of control systems were used in the vortex encounter simulation to determine the feasibility of using some form of automatic control to alleviate vortex induced upsets. For comparison purposes, bare airplane (controls fixed) encounters, and encounters with a human pilot model were also run. Further, the effects of "slow" and "fast" acting actuators on upset severity and recovery strategy was explored (and found to be significant).

A. AUTOMATIC CONTROL SYSTEMS

The several types of automatic control systems considered were:

Rate Command System

With this system only pitch rate, yaw rate, and roll rate feedbacks were used.

Attitude Command Systems

Two types of attitude systems were considered. One with pitch attitude (and rate), bank angle (and rate), and yaw rate feedbacks; and one with a heading feedback in addition. These two types of attitude command systems were called "bank angle command" and "heading command" systems, respectively.

In defining the specific automatic control systems for the PA-30 and the CV-880, two different approaches were taken. Command augmentation systems had already been designed and flight tested in a PA-30 aircraft at the NASA Flight Research Center (Ref. 6). Those systems were used as a starting point and modified primarily by increasing rate feedback gains for this study. The resulting bank angle command system is shown in Fig. VI-1.

New command augmentation systems were designed in this study for the CV-880. Figures VI-2a and VI-2b present composite lateral and longitudinal block diagrams for the control systems used with the CV-880 (i.e., rate command, bank angle command, and heading command systems).

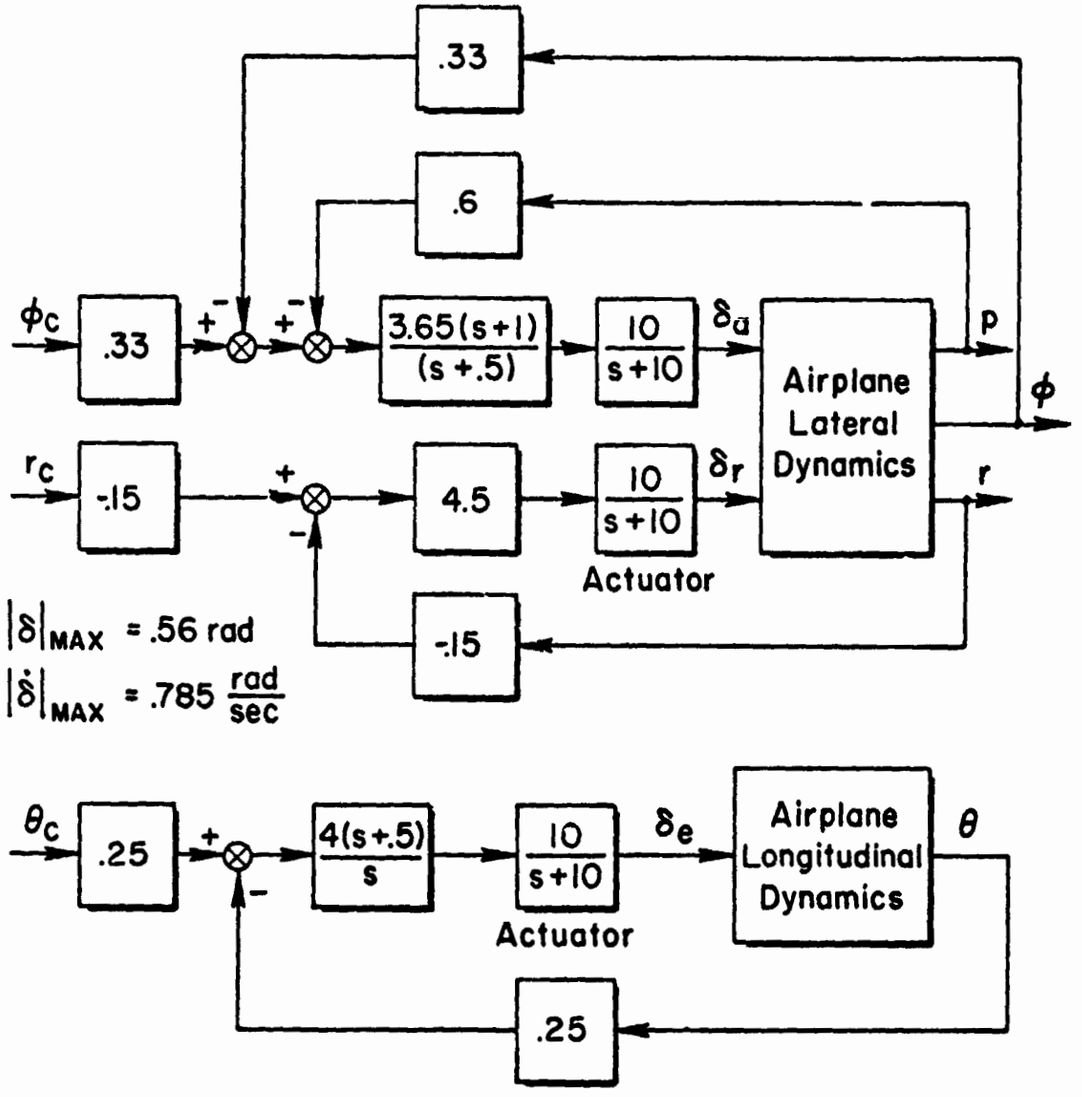

Figure VI-1. Bank Angle Command System for PA-30

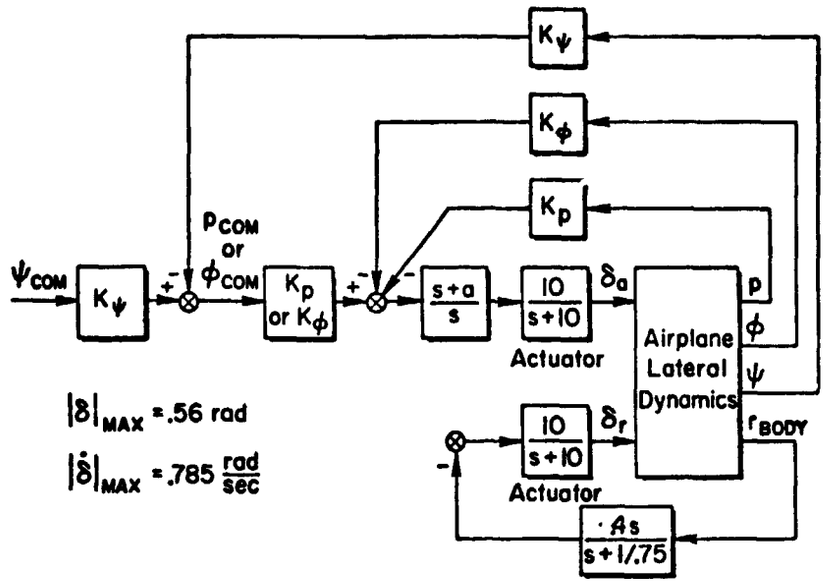

Rate Command System	Bank Angle Command System	Heading Command System
K_p = .25	K_p = 2.0	K_p = 2.0
K_ϕ = 0	K_ϕ = 3.4	K_ϕ = 3.4
a = 4.0	a = .01	a = .01
K_ψ = 0	K_ψ = 0	K_ψ = 2.818

Figure VI-2a. Lateral Block Diagram for CV-880 Control Systems

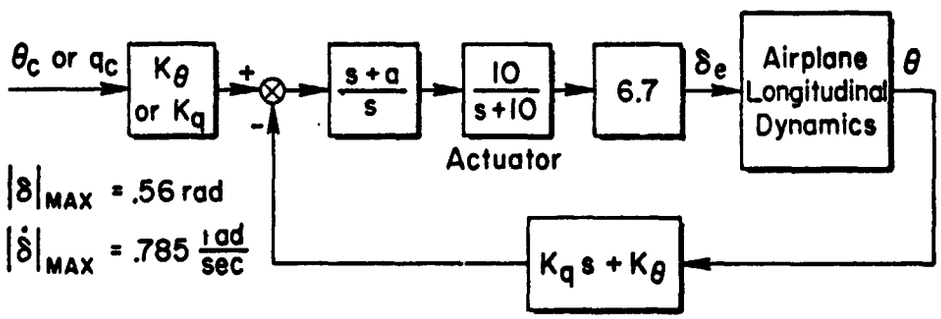

Bank Angle and Heading Command Systems	Rate Command System
K_q = -.5	K_q = -.4
K_θ = -.95	K_θ = 0
a = .6	a = 2.5

Figure VI-2b. Longitudinal Block Diagram for CV-880 Control Systems

Due to the relatively low aileron control power available for the PA-30 (compared to the vortex strength used) full aileron was required to minimize the bank angle during an upset. The proper control strategy thus resembled that of a bang-bang system until the bank angle and roll rate were both relatively small. However, a bang-bang aileron position could not be achieved due to the low rate limit initially used for the aileron actuator. This resulted in a lag between the commanded aileron and the actual aileron position. To compensate for this lag the roll rate gain was increased to a value that would typically be considered as higher than normal. The identification of such an "abnormal" system characteristic as being desirable in some situations for minimizing vortex upsets was one of the goals of the study.

Subsequent to the initial analyses and control system designs, some up-to-date PA-30 control surface data was obtained. Thus, the actuator lag time constant was decreased from 1/10 to 1/30 sec and the aileron rate limit was raised from 45. deg/sec to 120. deg/sec. These two changes resulted in a much more rapidly responding aileron, thereby making unnecessary (and undesirable) the very high roll rate gain previously required for a good system. Block diagrams of the "new" bank angle command system are presented in Fig. VI-3.

While on the subject of desirable and undesirable control system characteristics, it is pertinent to note than an aileron to rudder crossfeed is a very undesirable feature to have when encountering a vortex at a glancing angle. The purpose of such a crossfeed is typically to reduce sideslip due to aileron. However, when encountering a strong vortex at a glancing angle it is common for the airplane to develop an appreciable initial yawing in the direction opposite to that of the rolling motion. Thus, aileron opposing the roll will produce rudder to exaggerate the yawing (and sideslip). This is particularly bad when vortex induced sideslip is large to begin with.

B. HUMAN PILOT MODEL

Initially it was hoped to develop separate pilot models for "surprised" and "expectant" pilot situations. These labels refer to the pilot's degree of surprise at encountering a vortex wake. However, the development of a surprised pilot model was found to be beyond the scope of the project goals

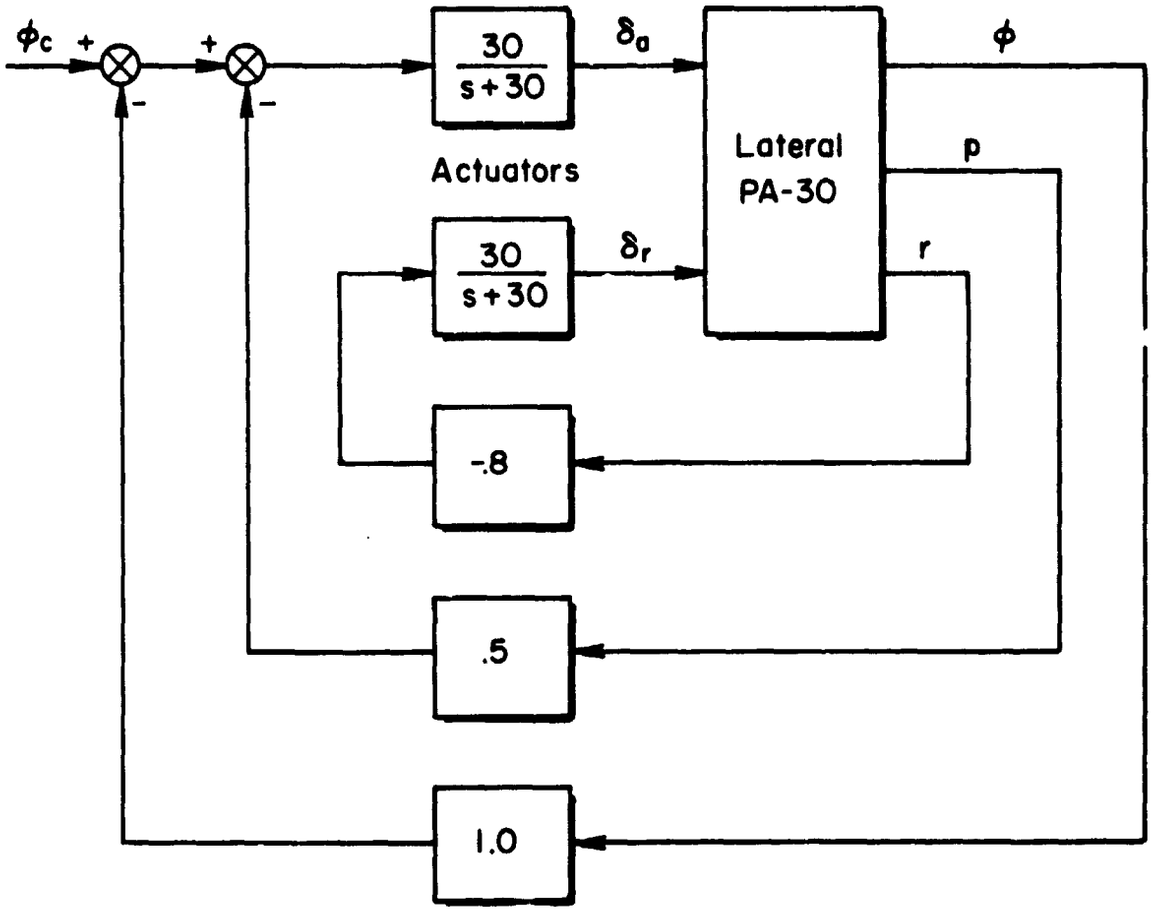

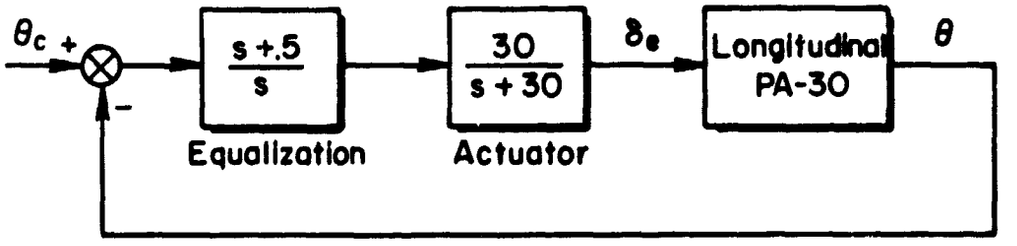

Figure VI-3. PA-30 Longitudinal and Lateral Block Diagrams for Configuration with Higher Bandwidth Actuators (Called Bank Angle Command System)

and was therefore not pursued. Our analysis showed that human pilot control of the rudders would require considerable attention and yet would not produce sufficient performance improvement to warrant his effort. Thus, it was assumed (for simulation purposes) that he would adopt a "feet on the floor" strategy. Further, because the more interesting variables during a vortex upset are lateral-directional in nature, it was decided to utilize the automatic longitudinal pitch attitude controller for all of the human pilot vortex encounters. This also tended to simplify the various upset comparisons. As a consequence of all this, the human pilot model used in the simulation (representing the expectant situation) was confined to roll axis control. Further discussion of human pilot modeling attempts using flight test data is included in Appendix D.

The specific pilot model used is one with a gain, lead, and time delay as shown in Eq. VI-1 (Ref. 9).

$$Yp_{\varphi} = K_{\varphi}[s + (1/T_L)]e^{-\tau_a s} \qquad \text{(VI-1)}$$

Typically, the lead (T_L) will be the same magnitude as the airplane roll-subsidence time constant (T_R), and the time delay (τ_a) is about .33 sec.

For comparison purposes an automatic yaw damper was included in some of the simulated vortex encounters to give the human pilot a better handling vehicle to control. This yaw damper was the same one used in the automatic bank angle command system. With this augmented airplane the recoveries from large upsets were much smoother than when the human pilot model was controlling the bare airplane. Time traces of upsets will be seen in a later section.

C. HANDLING QUALITIES CONSIDERATIONS

A concise evaluation of the handling qualities aspects of the "initial" bank angle command system on the PA-30 is given in Appendix C. Although the handling qualities criteria used there were developed for a different situation (not an attitude command system), they do represent the only known data. Based on these available criteria the net result of the evaluation in Appendix C is that the bank angle command system designed to minimize vortex encounter upsets is expected to result in favorable pilot opinion for normal flight operations.

SECTION VII

TYPICAL TIME TRACES OF VORTEX ENCOUNTERS

In this section a sampling of time traces for various simulated vortex encounters is presented. The traces included here were selected because they exhibit features considered pertinent in making a point or drawing a conclusion. It is noted that the specific encounters selected are not isolated cases that exhibit unique features in some way or other (although that too would be of interest), but instead are considered typical representations of whatever point is being made.

A. 90 DEG INTERCEPTS (ENCOUNTERS PERPENDICULAR TO THE VORTEX AXES) WITH THE PA-30 BEHIND A JETSTAR

For this type of encounter the vortex flow appears as a rapid sequence of up and down flows as each vortex is penetrated. Consequently, the most pertinent variable to consider is the normal acceleration. Most other variables have very little excitation because the encounter is over so quickly. In fact, the entire "upset" is over before any effective control action can be achieved. As a result, the bare airplane response looks just like the response with either a rate feedback control system or an attitude feedback control system, as can be seen in Figs. VII-1, VII-2, and VII-3. For comparison purposes, Figure VII-4 shows the normal acceleration and pitch rate traces that were measured in a flight test situation of an F-111 aircraft penetrating the wake of a C-5A. The qualitative similarity is quite evident, although the numerical values are not the same (nor would they be expected to be).

B. 90 DEG INTERCEPT WITH CV-880 BEHIND A C-5A

Figure VII-5 shows a simulated vortex encounter of a CV-880 behind a C-5A. For this case the motion of the airplane as it passes from one vortex to the other is even less significant than it was with the PA-30 encounters, as evidenced by the normal acceleration trace being more symmetric. (Notice that the normal acceleration looks like the vertical flow that would be sensed by an inertially referenced probe moving laterally across the wake.)

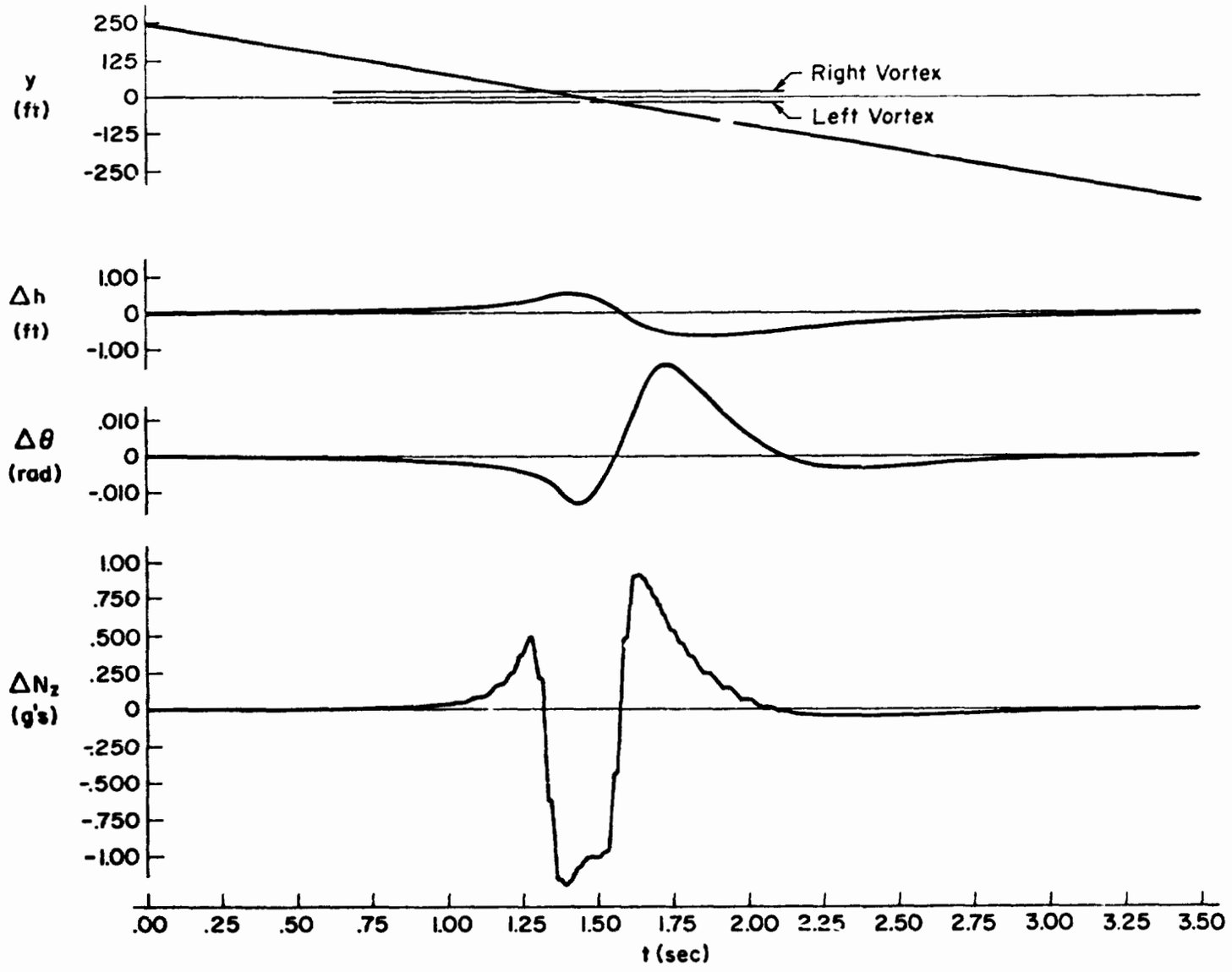

Figure VII-1. PA-30 Bare Airplane Flying Through Jetstar Vortices from Right to Left; $\gamma_o = 0$; $V_{T_o} = 174$ ft/sec; $z_o = 0$; $y_o = 250$ ft; $\psi_o = -90^o$

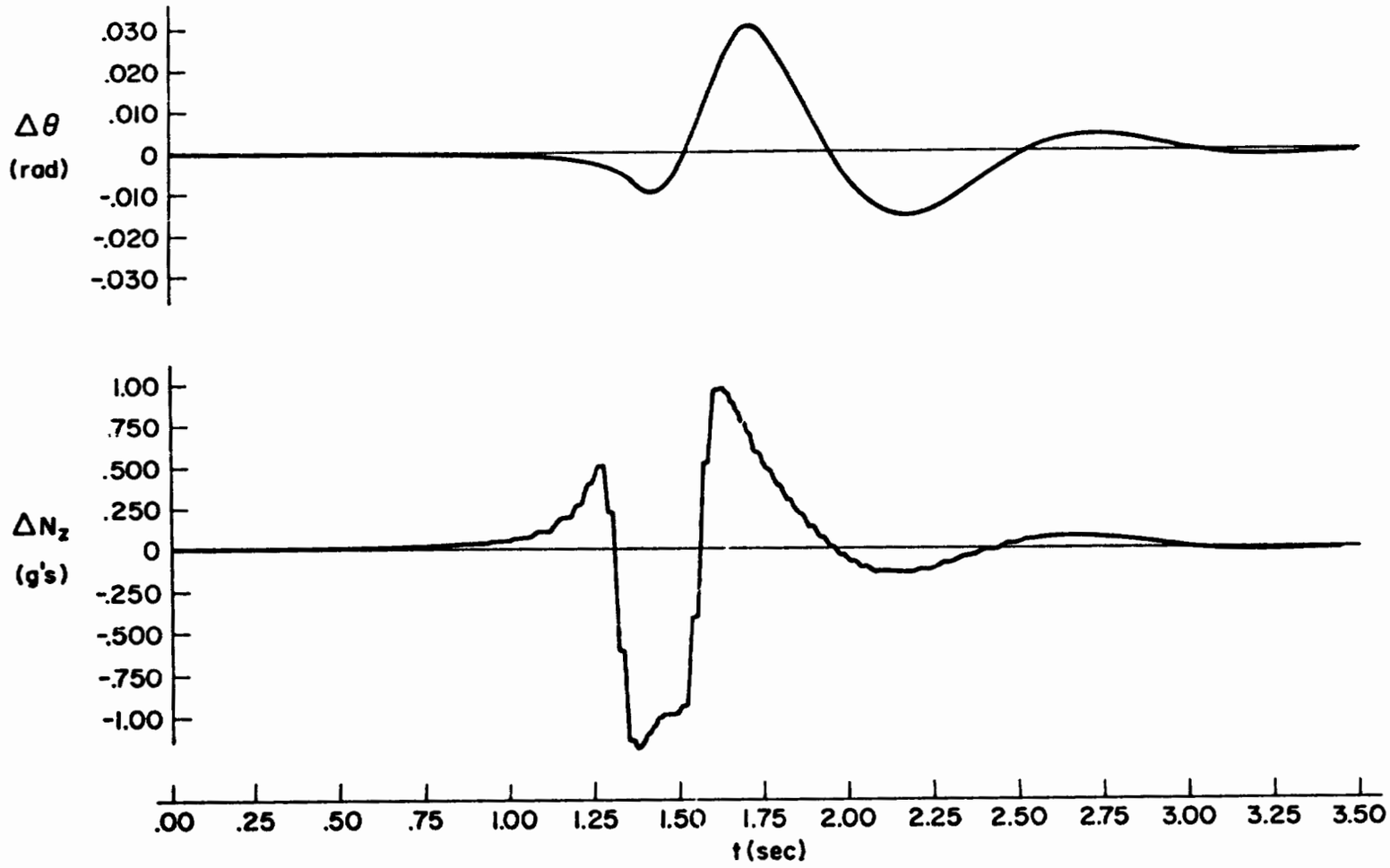

Figure VII-2. PA-30 With Rate Control System Flying Through Jetstar Vortices from Right to Left;
$\gamma_o = 0$; $V_{T_o} = 174$ ft/sec; $z_o = 0$; $y_o = 250$ ft; $\psi_o = -90^\circ$

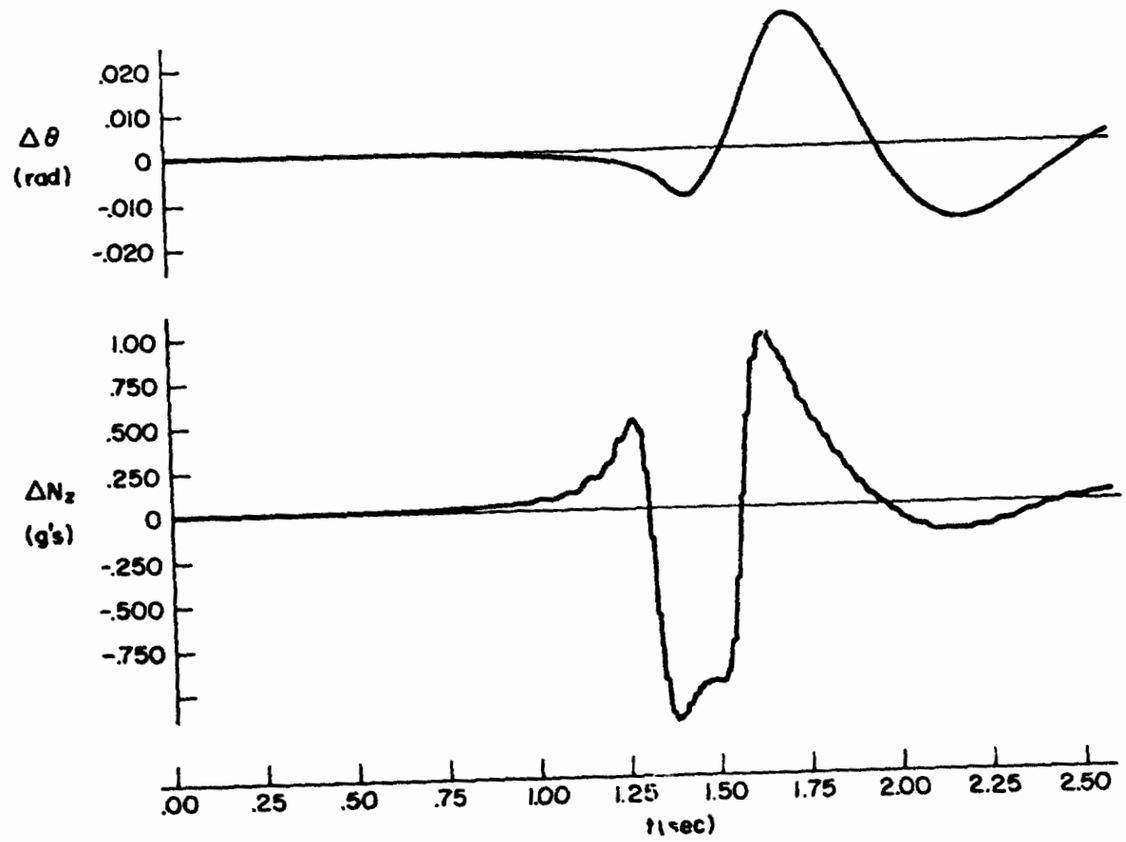

Figure VII-3. PA-30 with Attitude Control System Flying Through Jetstar Vortices from Right to Left;
$\gamma_o = 0$; $V_{T_o} = 174$ ft/sec; $z_o = 0$; $y_o = 250$ ft; $\psi_o = -90^\circ$

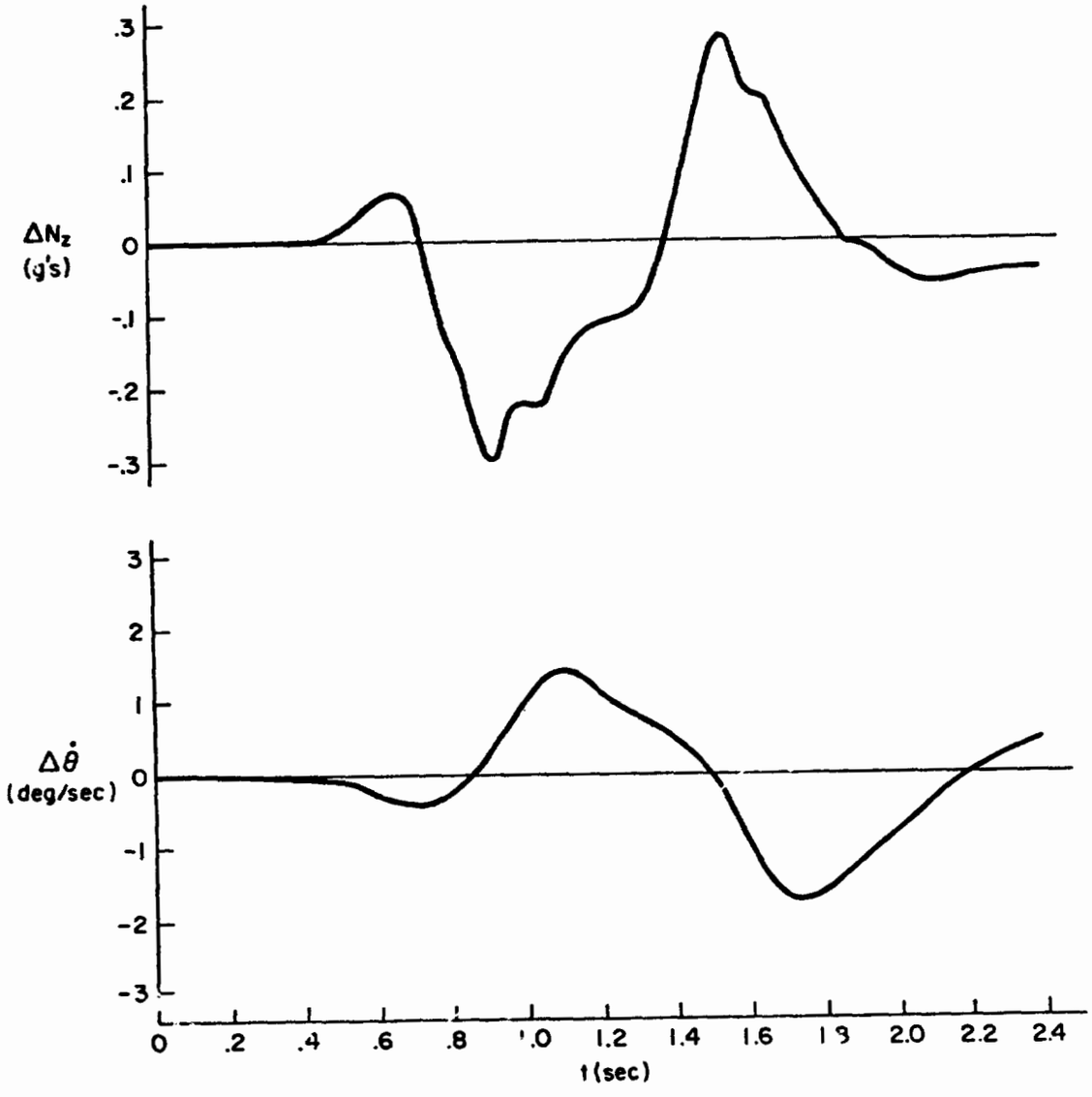

Figure VII-4. Flight Data of F-111 Penetration Perpendicular to Vortex Wake of C-5A

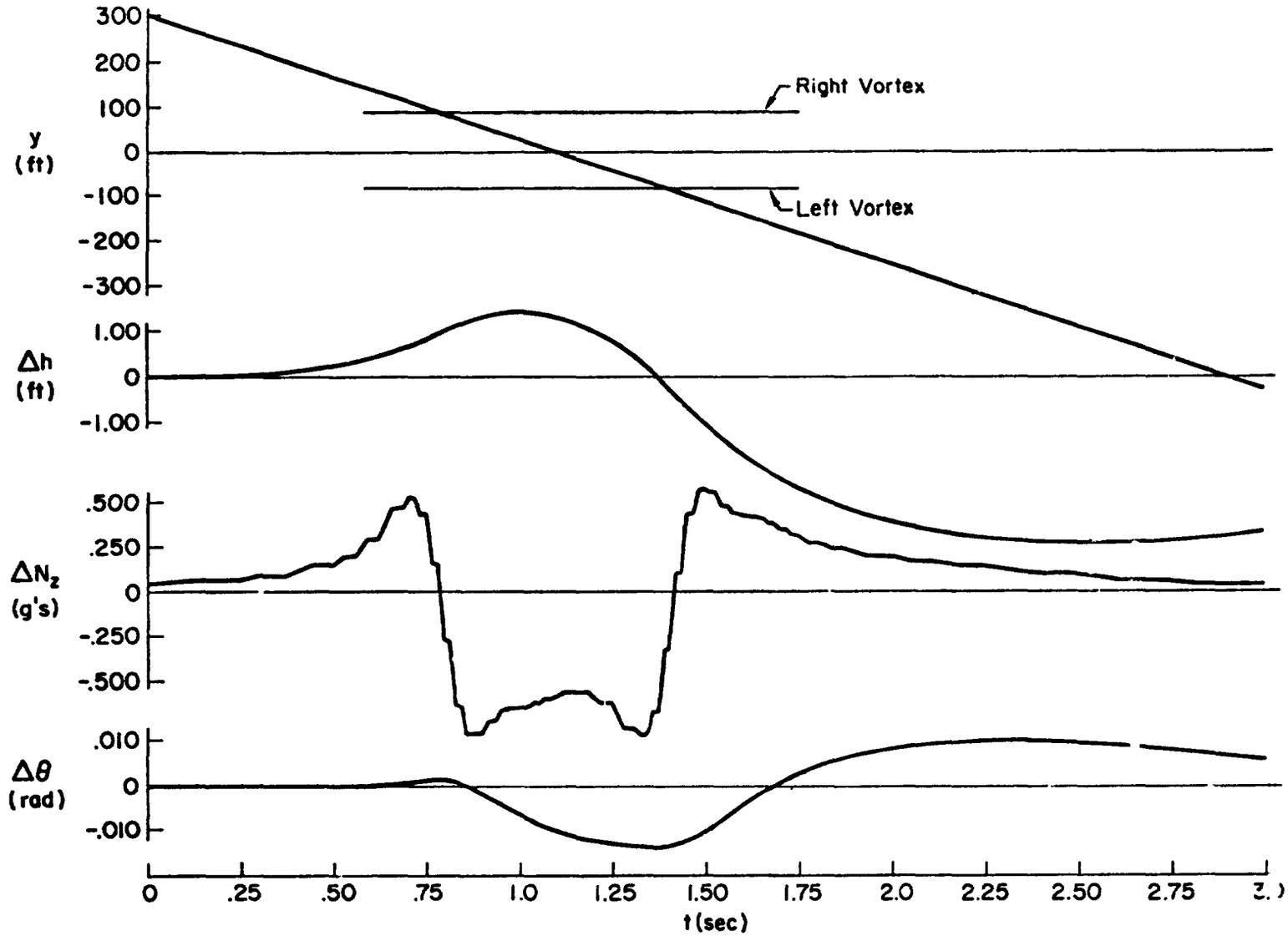

Figure VII-5. CV-880 Bare Airplane Flying Through C-5A Vortices from Right to Left; $\gamma_o = 0$; $z_o = 0$; $y_o = 300$ ft; $\psi_o = -90°$

C. 9 DEG GLANCING INTERCEPT FROM SIDE WITH PA-30 BEHIND A JETSTAR

Figure VII-6 shows the time traces for a controls fixed glancing encounter from the side. While it can be seen that the primary variable of interest is bank angle, it is noted that there is more normal acceleration than one might typically expect for such a glancing encounter.

The bank angle trace shows the airplane to be first banking to the right as the left wing enters the upflow region of the right vortex, and then rolling over rapidly to the left as the center of the vortex is hit. This reversal in bank angle is characteristic of glancing encounters from the side, and can "trick" a pilot into applying aileron in the same direction as the vortex is ultimately rolling him. Just such a situation is likely to have occurred in the 1972 fatal crash of a DC-9 behind a DC-10 at Greater Southwest airport in Fort Worth. In that situation an initial roll in one direction was followed by a large roll (90^{o}) in the opposite direction, and then ground contact shortly thereafter.

D. MISCELLANEOUS GLANCING ENCOUNTERS FROM BELOW

Figures VII-7, VII-8, VII-9, VII-10, and VII-11 show glancing encounters from below a vortex. When a vortex is encountered from below the rolling moment is continuously in the same direction (rather than reversing) thereby giving larger peak bank angles. These five example vortex encounters for a 3 mile separation are presented to show the details of the upsets with and without augmentation systems. Figures VII-7 and VII-8 shows the PA-30 and CV-880 without augmentation systems. Figure VII-9 shows a PA-30 with a bank angle command system. Figures VII-10 and VII-11 then show a CV-880 with heading command, and bank angle command systems, respectively. Roll rate command systems are not shown because they were not very effective in alleviating the upsets.

Figure VII-7 shows that the PA-30 rolls inverted when no control is applied. It also shows that the peak yaw rate occurs at about the time the vortex center is reached. However, the interesting aspect of the peak yaw rate is the direction of yawing. The vortex is rolling the airplane to the left, but yawing it to the right. Thus, the encounter produces an uncoordinated situation wherein the motion cues could be confusing to a pilot.

Figure VII-8 shows the CV-880 response to a vortex encounter when no control is applied. It is qualitatively similar to the PA-30, including the uncoordinated yawing, but the maximum bank angle is less.

Figure VII-9 shows that for the PA-30 with a bank angle command system the aileron position limit is reached prior to encountering the center of the vortex. The bank angle trace shows the airplane rolling over to about 60 degrees in 2-1/2 seconds, and then rolling back to wings level in another 2 seconds. Notice that even though the aileron position and rate limits were reached, roll control is quite good once the central region of the vortex is passed.

Figure VII-10 shows an interesting point to be considered with regard to the useful control system feedback variables. In this situation the CV-880 has a heading feedback as well as a bank angle feedback to the aileron. Due to the large adverse yaw, the aileron command due to heading subtracts from the aileron command due to bank angle. (The traces show ψ and φ to be very similar, but with opposite signs.) Thus, the net aileron command is quite small even though the bank angle is about 35 degrees. This is not a good situation. During a vortex upset the control of bank angle is more important than maintaining a given heading. In fact, better heading control will ultimately be realized if good bank angle control is achieved. The conclusion to be drawn here is that a heading feedback to the aileron is detrimental to good bank angle control.

Figure VII-11 shows the traces for a control system that is the same as that used in Fig. VII-10, except for the removal of the heading feedback. This system is called a bank angle command system. Here it is readily seen that the bank angle never builds up, and the maximum heading change is actually about the same as that found using the heading command system! This is clearly a better system for controlling vortex wake upsets.

A similar situation to the above example (of the detrimental effect of a heading feedback) was found when an aileron-to-rudder crossfeed was used. Again, due to the opposite (or adverse) roll and yaw directions resulting from the vortex flow, the direction of the rudder from the crossfeed tends to <u>increase</u> the yawing excursions, and makes any upset considerably worse.

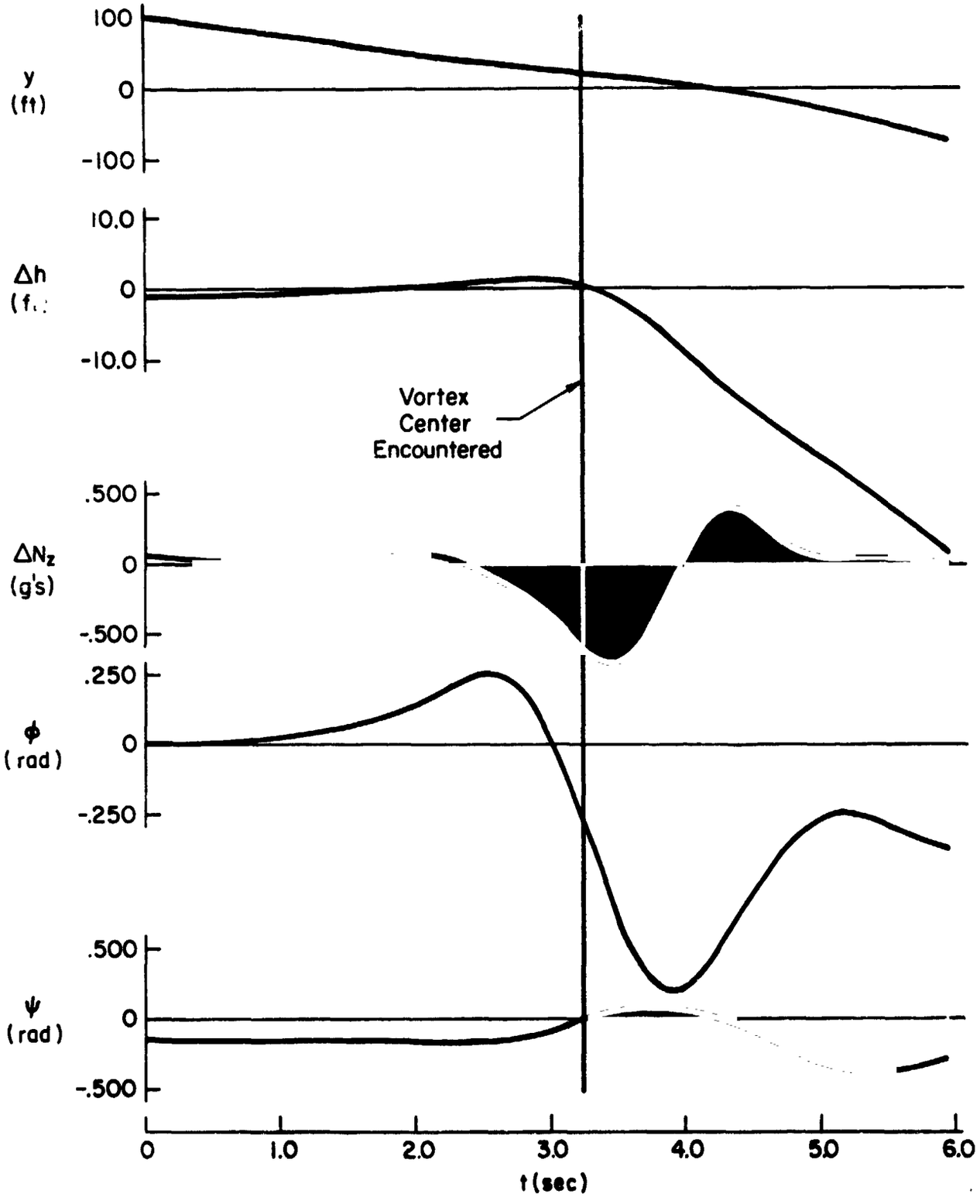

Figure VII-6. PA-30 Bare Airplane Flying Through Jetstar Vortices from Right to Left; $\psi_o = -9^o$; $\gamma_o = 0$

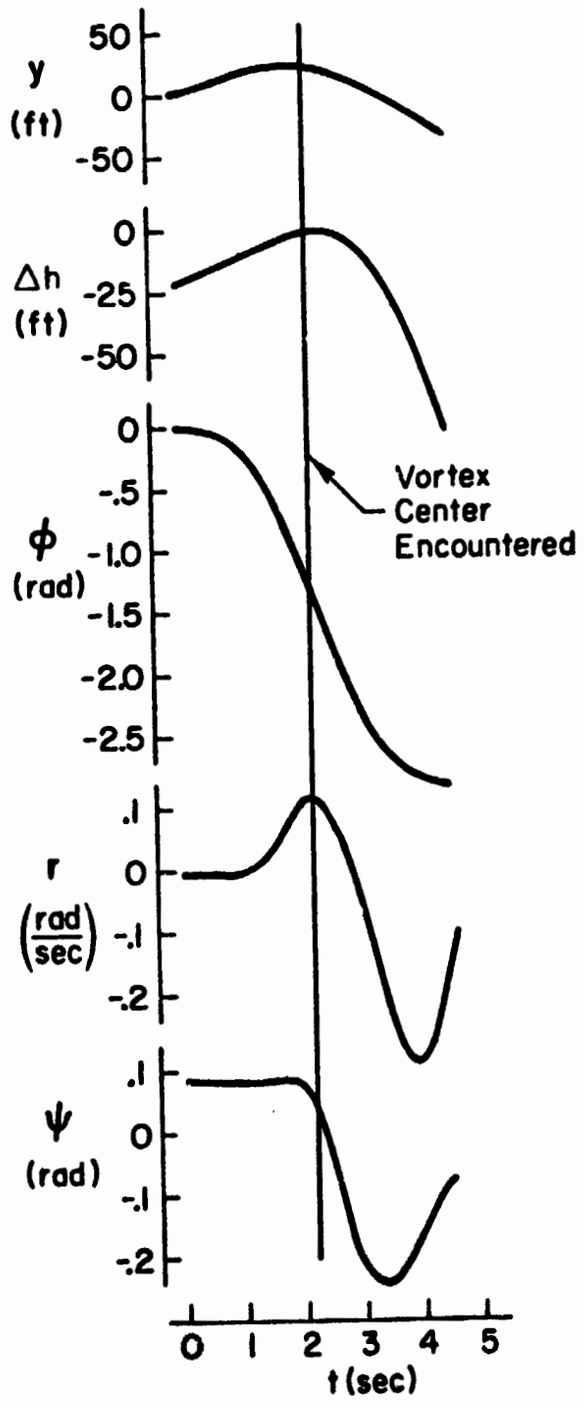

Figure VII-7. PA-30 Bare Airplane; 3 Mile Separation Behind Jetstar

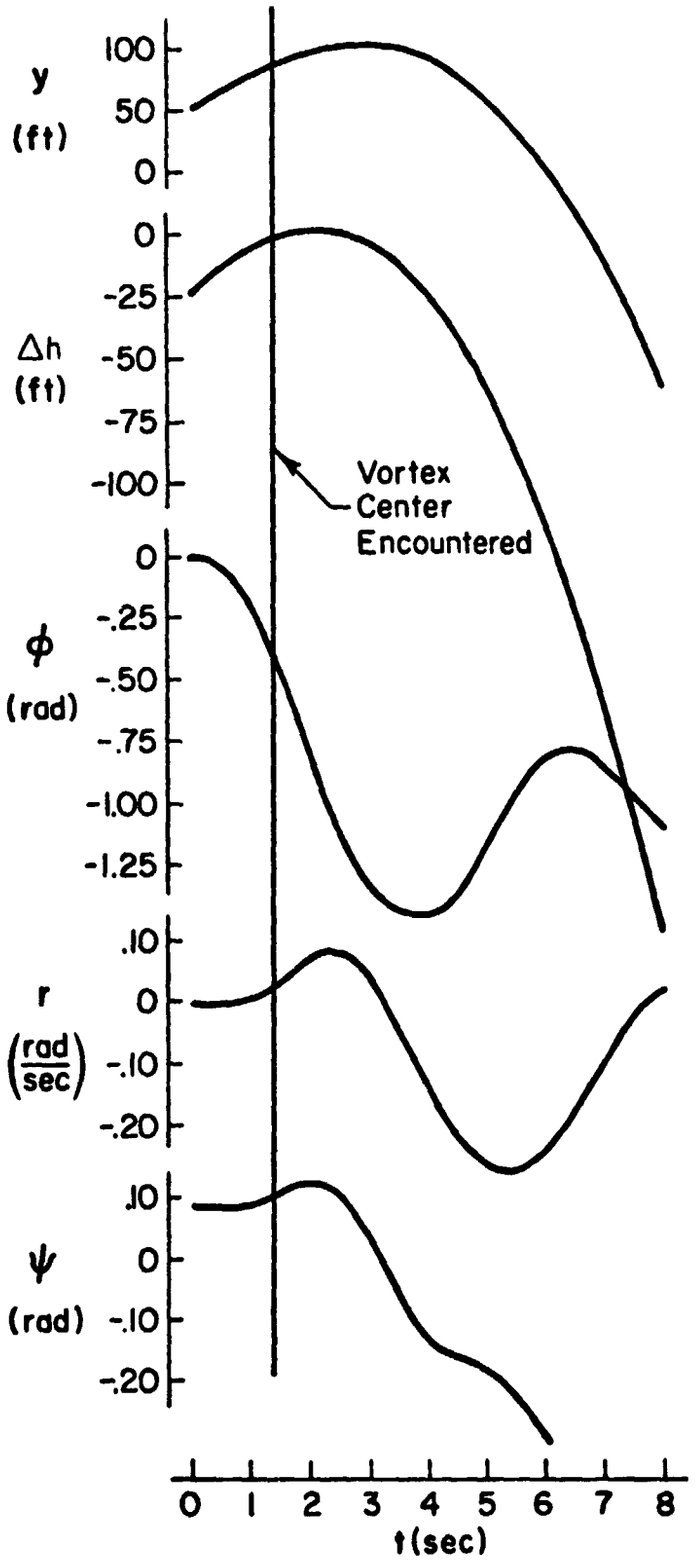

Figure VII-8. CV-880 Bare Airplane; 3 Mile Separation Behind C-5A

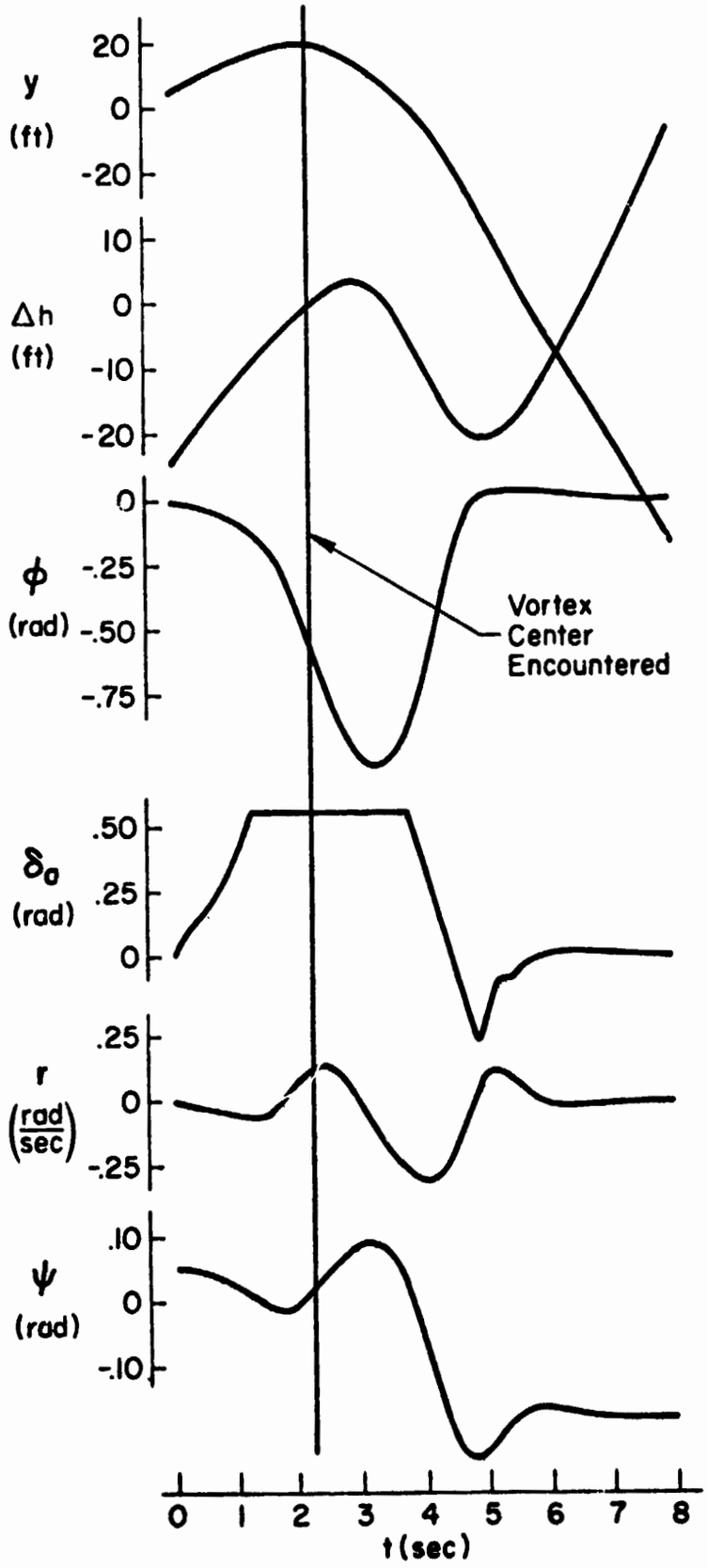

Figure VII-9. PA-30 Bank Angle Command System; 3 Mile Separation Behind Jetstar

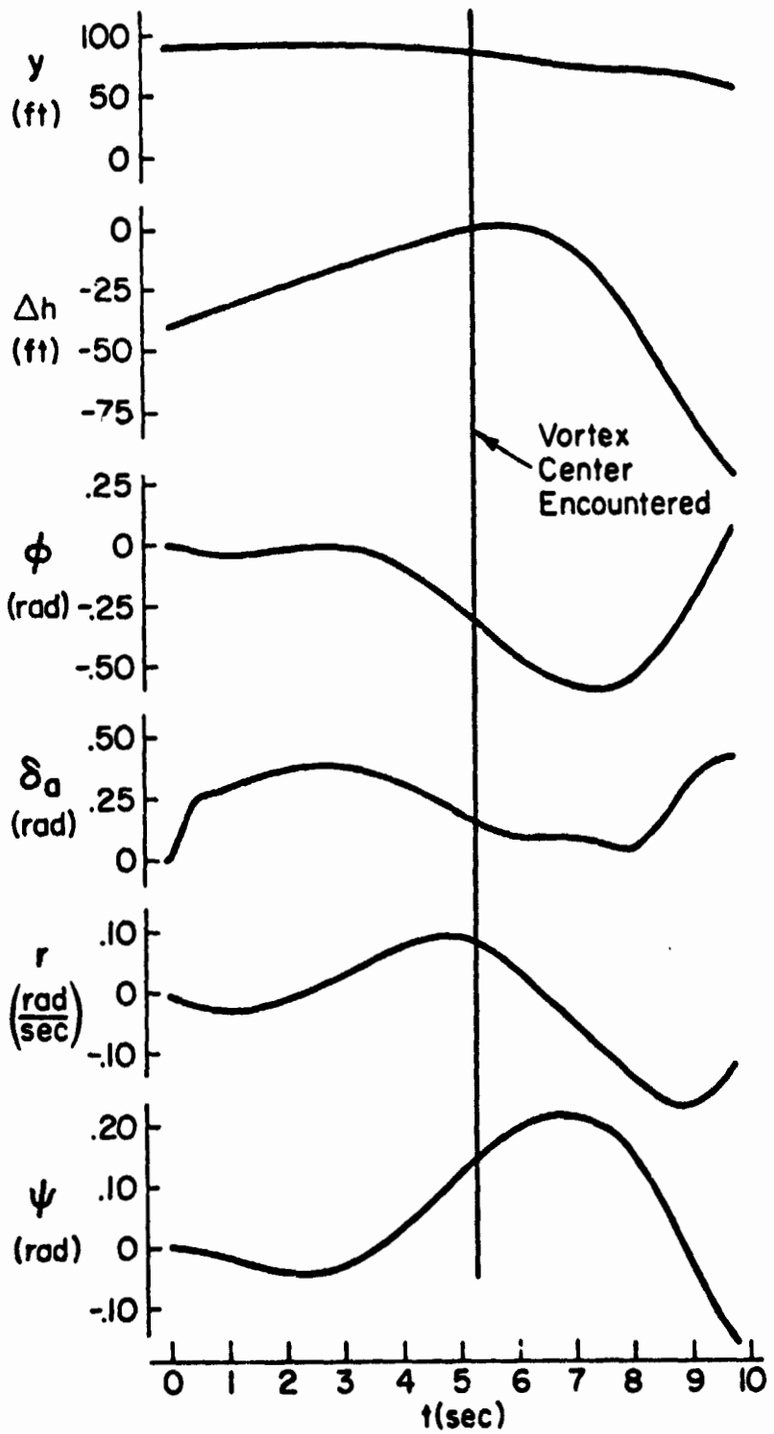

Figure VII-10. CV-880 Heading Command System;
3 Mile Separation Behind C-5A

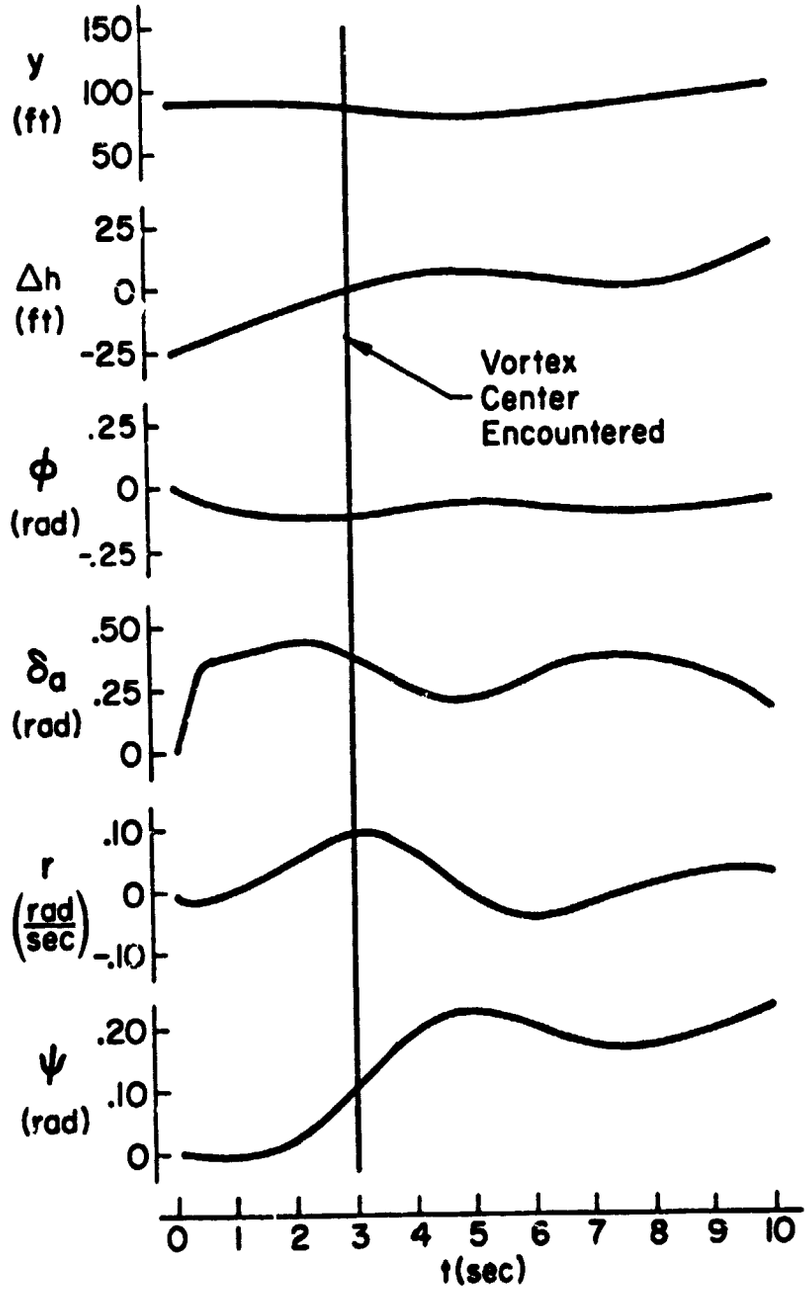

Figure VII-11. CV-880 Bank Angle Command System;
3 Mile Separation Behind C-5A

Thus, another conclusion regarding control system effectiveness in alleviating vortex encounter upsets is that an aileron to rudder crossfeed is detrimental.

E. MAXIMUM BANK ANGLE COMPARISONS

The key performance metric for evaluating glancing vortex encounter upsets is the maximum bank angle experienced. Tables VII-1 and VII-2 present a summary of maximum bank angle comparisons for several types of control systems on the two example aircraft considered.

TABLE VII-1

GENERAL AVIATION AIRCRAFT PENETRATING EXECUTIVE JET TRANSPORT WAKE FROM BELOW

Maximum Bank Angle Comparison

	SEPARATION	
	3 Mile	10 Mile
No Augmentation System	180°	105°
Bank Angle Command System	60°	23°

TABLE VII-2

COMMERCIAL JET TRANSPORT PENETRATING JUMBO JET TRANSPORT WAKE FROM BELOW

Maximum Bank Angle Comparison
(3 Mile Separation)

No Augmentation System	90°
Heading Command System	35°
Bank Angle Command System	7°
Roll Rate Command System	25°

As can be seen in the comparisons in the tables, the automatic control systems provide a significant reduction in the maximum bank angle experienced in a vortex wake upset for both types of aircraft.

F. COMPARISON OF HUMAN PILOT AND AUTOPILOT CONTROL

So far, no human pilot control has been considered. As a separate phase of the study, comparisons were made with identical vortex encounters using models for manual and automatic control. For these encounters the vortex model parameters used were different from those used up to this point. They were obtained by adjusting the vortex model parameters (given in Section II) to fit tower data from a B-727 flyby at NAFEC (see Appendix A). Another significant difference exists in the situations that follow. The bandwidths of the control surface actuators have been increased. This was done to reflect the latest information on the actual hardware on NASA's PA-30. The actuator time constants were decreased and the rate limits on the surface motion were increased. The consequences of these changes were presented in Section VI, but it is mentioned here to remind the reader that the traces that follow are not to be directly compared with those that have already been presented.

Figures VII-12 and VII-13 show vortex encounters (PA-30 behind a B-727) from the side and from below, respectively, for several types of control. As can be seen, the bank angle command system does a better job than the human pilot in controlling the upset. But the primary difference is not so much in the attenuation of the peak bank angle as it is in the damping out of subsequent motions due to the dutch roll mode. This suggested that a yaw damper might be very useful to the human pilot. Thus, the same human pilot along with the yaw damper from the bank angle command system was tried. It can be seen that the human plus yaw damper does just about as good a job as the fully automatic system. It must be remembered, however, that the human pilot model used here always puts in control in the correct direction, and without large delays due to surprise, confusion, incapacitation (due to large vortex-induced jostling), etc. Thus, any comparisons are based on the human pilot behaving in the most favorable manner possible — rather than

in a "typical" manner. Clearly it would be desirable to get further comparisons to verify these conclusions. Such comparisons might be obtained in a moving-base simulator.

It is noted that the bare airplane entering the vortex from below is upset in a very interesting way. It turns out to be performing a "split-S" maneuver in that it is rolled over 180 degrees onto its back, and then it dives through the vertical and pulls up again. (The pitch trace is not included here, but it looks approximately like a ramp down to −90 degrees, followed by a ramp back up.) The bank angle and heading traces both show the required 180 degree jumps as the airplane passes through the vertical.

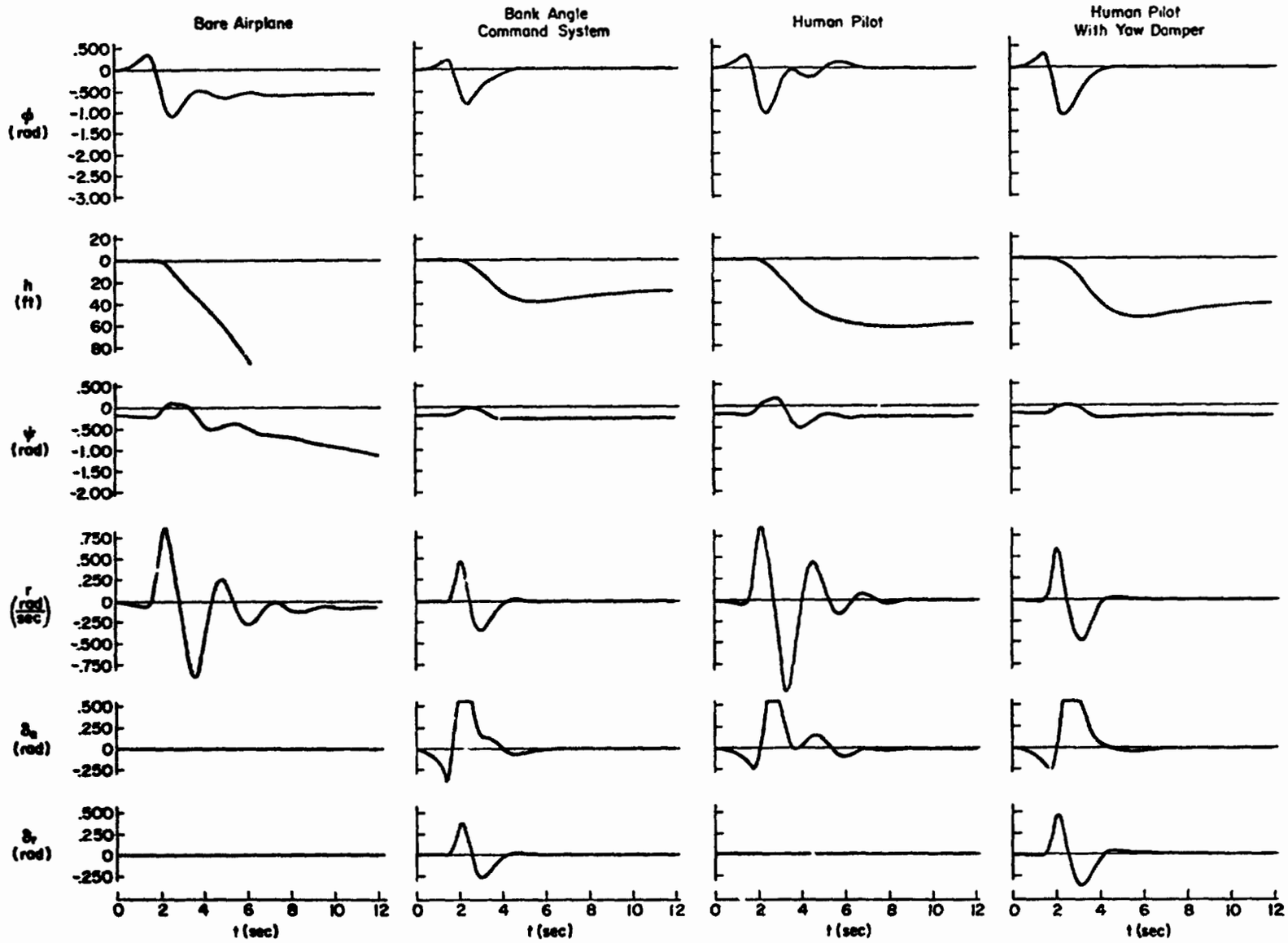

Figure VII-12. Example Vortex Encounters from the Side (PA-30 Behind B-727) for Several Types of Control

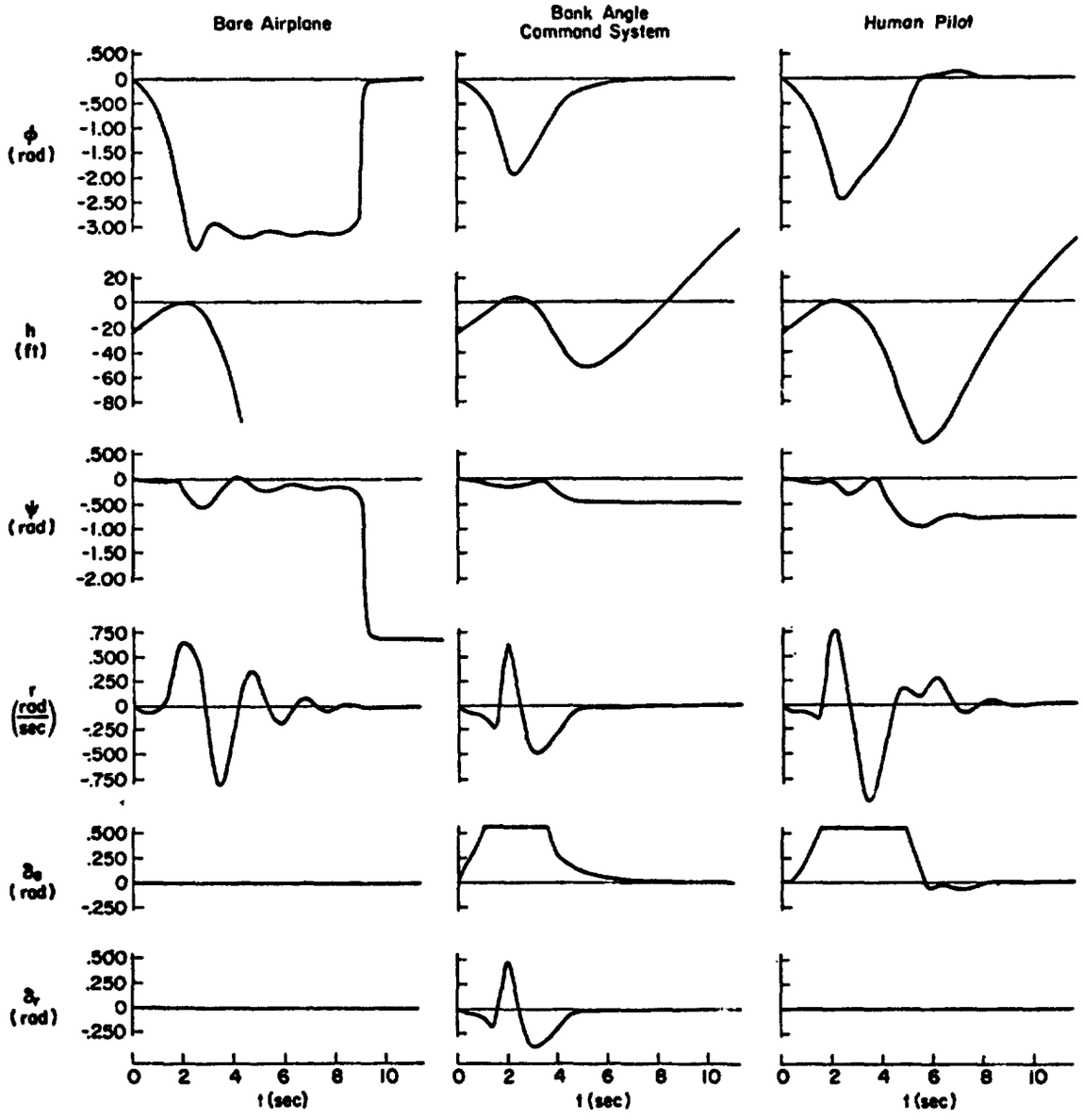

Figure VII-13. Example Vortex Encounters from Below (PA-30 Behind B-727) for Several Types of Control

SECTION VIII

SENSITIVITY OF UPSET TO VORTEX PARAMETERS

Several questions need to be answered with regard to how well the vortex flow needs to be known (and modeled) to insure valid simulation results. The first question concerns the analytical form of the vortex model to be used. Then, the questions of how accurate each parameter in the model needs to be known, and what are the effects of errors in these parameters. Before attempting to answer these questions, the results of some simulated encounters with varying vortex flow characteristics will be presented. Then answers to these questions will be noted, along with some guidelines concerning future full scale vortex flow measurements.

The vortex model used in this report has three basic characteristics (core diameter, maximum tangential velocity, and total circulation) which are related by the following equation (see Appendix A).

$$\Gamma_o = 4.40\, d_{CORE} V_{\theta_{max}} \qquad \text{(VIII-1)}$$

This shows that there are only two flow characteristics that can be varied independently.

To determine the effects of change in these flow characteristics a base case of vortex parameters was chosen, and systematic parameter changes were made. Simulated vortex encounters with identical initial conditions were run and the changes in the upsets noted. The base case was chosen to be a fit to the B-727 tower data shown in Appendix A. This was

$$\frac{\Gamma_o}{2\pi} = 250.\ ft^2/sec \qquad \text{(VIII-2)}$$

$$d_{CORE} = 1.7\ ft \qquad \text{(VIII-3)}$$

$$V_{\theta_{max}} = 209.\ ft/sec \qquad \text{(VIII-4)}$$

The first perturbations were to double the core diameter while holding the maximum velocity fixed, and to double the core diameter while holding the circulation fixed. These two perturbation cases (along with the base case) allowed three comparisons to be made. Namely, the effects of separately holding circulation, core diameter, and maximum velocity constant (while varying the other two parameters).

The results of these comparisons were quite straightforward. When circulation was held constant, while core size and peak velocity were varied, the upsets (PA-30 with a bank angle command system) were essentially identical. However, when either core size or peak velocity was held constant the upsets were different — roughly in proportion to the resulting change in circulation (which was required to hold the appropriate parameter constant).

As a consequence of this observation more simulated encounters were run with circulation held constant, but with core size (and thus peak velocity) being varied by larger and larger amounts until the upset finally showed a change. This happened when the core diameter reached 13.6 ft (or about 1/3 of the wing span of the penetrating airplane). Figure VIII-1 shows a summary of the bank angle traces obtained during the encounters described above. Figure VIII-2 shows superimposed plots of the vortex flow (of the right side vortex) for the various core sizes, etc. looked at in this initial sensitivity investigation.

On looking at Fig. VIII-2 it is apparent why the upsets are essentially a function of only the circulation and are independent of the core size. The flow outside about a 4 ft radius is the same for all of the core diameters less than 7. ft (with circulation held constant). Thus, the flow over the major portion of the wing of the penetrating airplane is not much affected by core size differences. Further, the flow within the core (for the values of circulation and maximum velocity considered) is so large that stall is occurring on those strips within the core anyway (thus producing the same lift regardless of the flow magnitude differences). On the other hand, changes in the circulation are reflected in proportional changes in flow at all radii, and in particular, outside the core. Therefore, a scaling of upset magnitude with circulation is (by hindsight) obvious.

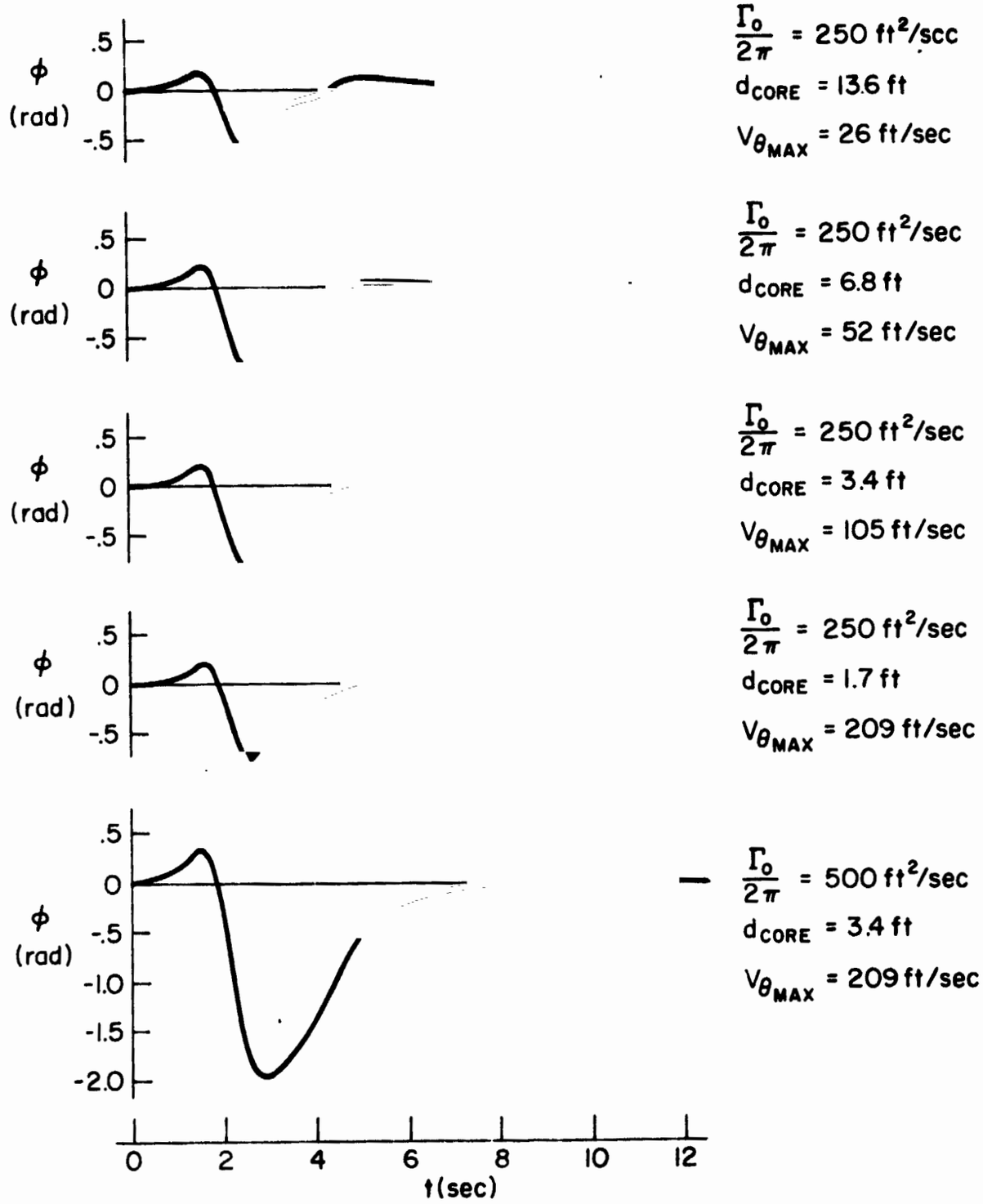

Figure VIII-1. Upset Comparisons for Various Vortex Parameter Values (Glancing Encounters from Right Side; $\psi_o = -10^o$, $\gamma_o = 0$)

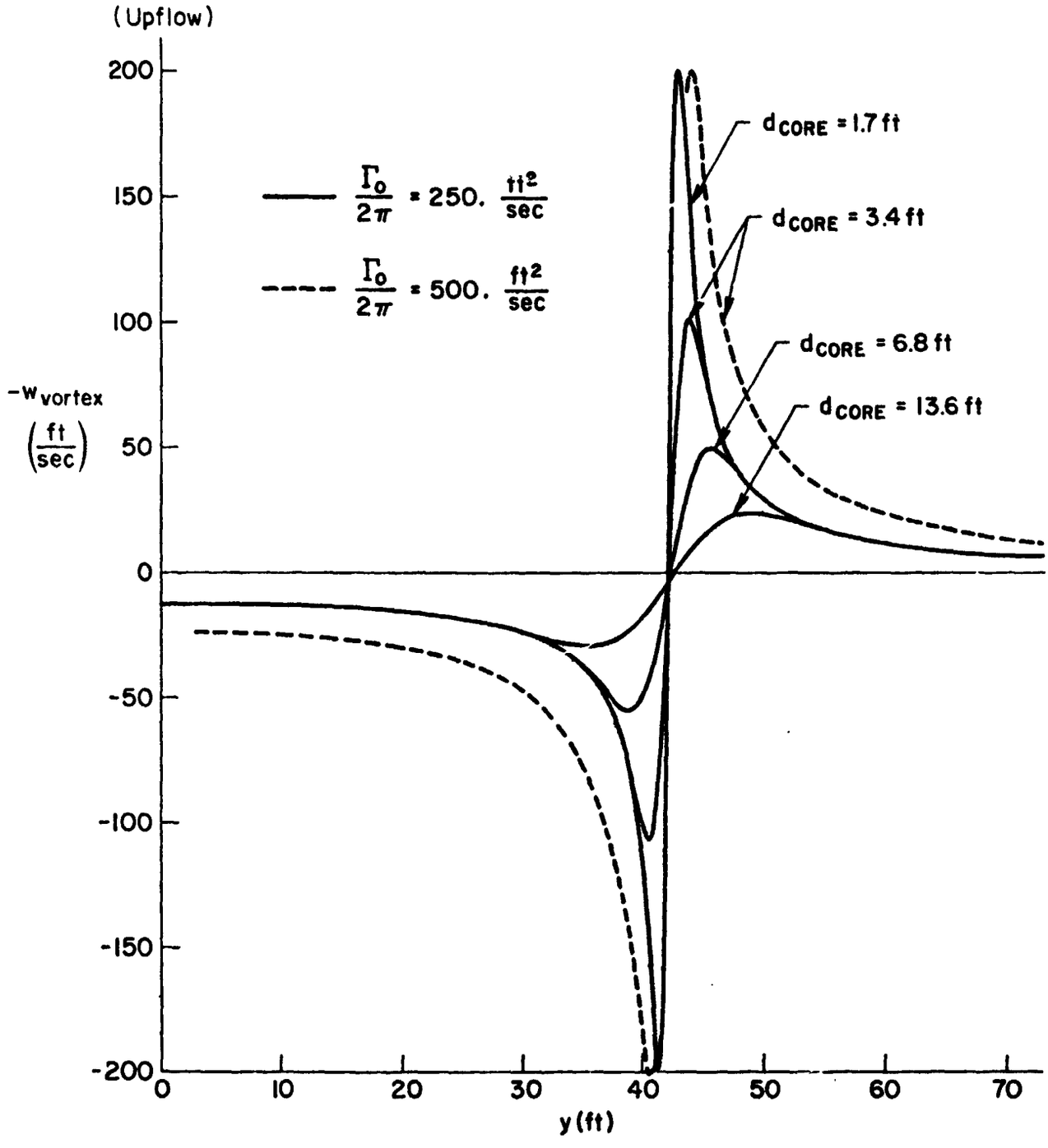

Figure VIII-2. Vortex Flow for Several Core Sizes and Vortex Strengths

Perturbations in vortex flow (as described above) were also tried with human pilot models controlling the PA-30. The results and conclusions are exactly the same as for the bank angle command system situation already presented.

Summarizing the upset sensitivity to vortex parameters, it appears that the details of the flow within the core have very little effect on the upset (for core diameters less than about 1/3 of the penetrating airplane's wing span). Thus, analytical vortex models that differ primarily in the description of flow within the core are for practical purposes equivalent models. The key parameter that needs to be accurately modeled is the total circulation, because the upset magnitude roughly scales with circulation. The implications for flow-measuring flight-test applications are clear. Determining only the maximum flow velocity, or the core diameter accurately is not very useful. Both need to be known in order to even estimate the circulation magnitude. Care should be taken to insure getting good measurements well outside the core to enable accurate estimates of the circulation to be made. Further simulation of upset comparisons should also be made to determine the effects of flow falloff with radius other than 1/r.

SECTION IX

SUMMARY OF RESULTS AND CONCLUSIONS

A six-degree-of-freedom nonlinear digital computer simulation was developed for analyzing the dynamic response of an airplane encountering a vortex wake. This simulation was used primarily to determine the feasibility of having an automatic control system to alleviate vortex encounter upsets. Secondary goals were concerned with better understanding the nature of the upsets and determining the conditions that lead to more hazardous upsets. A future use of the simulation might be to define a hazard volume along the final approach path at an airport. Based on the exercises of the simulation to date, the following is a listing of some of the general conclusions that can be drawn.

- A 90 deg vortex encounter gives a purely longitudinal situation with incremental normal acceleration (ΔN_z) being the largest effect.
- A vortex-induced ΔN_z can exceed the design loads of smaller encountering aircraft.
- 90 deg encounters with a PA-30 show the same general traces (and similar "kinks") of ΔN_z and $\dot{\theta}$ (pitch rate) as do flight data for an F-111.
- PA-30 results show that all control systems (SAS's) have nil effect in reducing the peak ΔN_z (for 90 deg intercept), and actually increase the peak $\Delta\theta$ (although it is still not large). The reason for this situation is that the encounter is over very quickly — before a SAS can do much. Thus, SAS and bare airplane results look alike.
- Glancing encounters produce primarily lateral disturbances (e.g., bank angle and sideslip), but sizeable pitch attitude and normal acceleration can still occur.
- The lateral situation is usually more critical than the longitudinal situation (and more amenable to alleviation of vortex induced upset via automatic control systems).
- The primary measure of a lateral upset is the maximum bank angle attained.

- Several conclusions were reached regarding the use of automatic control systems for alleviating vortex wake encounter upsets:
  - Specifically designed attitude command augmentation systems can provide significant alleviation of vortex wake upsets.
  - A rate damper or rate command system alone does not significantly alleviate vortex encounter upsets.
  - An "ideal" human pilot model (for roll control of an airplane with a yaw damper) can alleviate vortex upsets almost as well as an automatic system. (The pilot model is ideal in that it implicitly assumes the pilot always puts in control in the correct direction, and without large delays due to being surprised, confused, or incapacitated due to rapid motions.)
  - A heading to aileron loop is detrimental.
  - An aileron to rudder crossfeed is detrimental.
  - Control surface saturation (in rate or position) effects are important when trying to minimize separation distance, or when a small airplane is following a larger one. However, significant alleviation is still possible even with some saturation.
  - High authority and high surface rate limits are needed for a good vortex upset alleviating system.
  - If low bandwidth actuators are used, a good vortex upset alleviating system will differ from a conventional SAS in that it will have a higher roll rate gain and a lower bank angle gain than a conventional SAS would have.
  - If high bandwidth actuators are used, then a good vortex upset alleviating system is similar to a conventional SAS in loop structure and gains used.
- The characteristic of a vortex that has the largest effect on an encounter upset is the total circulation. In fact, the upset magnitude roughly scales with circulation; whereas the peak tangential velocity and the core size are individually not very important for core sizes less than about 1/3 of the penetrating airplane's wing span.
- Flow measuring test programs (whether wind tunnel, tower, or flight test) need to insure the simultaneous measurement of maximum flow velocity and core diameter in order to be able to estimate the circulation. Either quantity alone is not very useful.

- A summary of the items that vortex upsets are sensitive to include:
  - Vortex parameters (primarily the total circulation).
  - Vortex entry conditions (angle, direction, and duration near vortex center. It is possible to hit the center of a given vortex in several ways that give totally different upsets. Because of this it is tempting to classify a vortex as "non-hazardous" on the basis of flight encounters; whereas, in actuality, a different entry condition might produce a very large upset.)
  - Penetrating airplane geometry (wing span and aileron control power are key items).
  - Control surface actuator position and rate limits, and effective lag in actuation.
  - Control strategy during upset. (In human pilot cases can get delayed actions as well as wrong actions. Too high a gain along with a rate-limited control surface can take extra time to reverse a control input.)

REFERENCES

1. Robinson, Glenn H., and Richard R. Larson, A Flight Evaluation of Methods for Predicting Vortex Wake Effects on Trailing Aircraft, NASA TN D-6904, Nov. 1972.

2. Donaldson, Coleman duP., Richard S. Snedeker, and Roger D. Sullivan, Calculation of the Wakes of Three Transport Aircraft in Holding, Takeoff, and Landing Configurations, and Comparison with Experimental Measurements," FAA-RD-73-42, Mar. 1973.

3. Rose, R., and F. W. Dee, Aircraft Vortex Wakes and Their Effects on Aircraft," ARC CP No. 795, 1965.

4. NAFEC tower data for B-727. Forthcoming FAA report.

5. Von Mises, Richard, Theory of Flight, New York, Dover, 1959.

6. Loschke, Paul C., Marvin R. Barber, Calvin R. Jarvis, and Einar K. Enevoldson, Flight Evaluations of the Effect of Advanced Control Systems and Displays on the Handling Qualities of a General Aviation Airplane, SAE Paper 720316, SAE National Business Aircraft Meeting, Wichita, Kansas, Mar. 1972.

7. Nelson, Robert C., and Barnes W. McCormick, Aircraft-Vortex Penetration, SAE Paper 730296, SAE Business Aircraft Meeting, Wichita, Kansas, Apr. 1973.

8. Andrews, William H., Glenn H. Robinson, and Richard R. Larson, Exploratory Flight Investigation of Aircraft Response to the Wing Vortex Wake Generated by Jet Transport Aircraft, NASA TN D-6655, Mar. 1972.

9. McRuer, D. T., and E. S. Krendel, Mathematical Models of Human Pilot Behavior, AGARDograph No. 188, Jan. 1974.

10. "Flying Qualities of Piloted Airplanes," MIL-F-8785B(ASG), 7 Aug. 1969.

11. Ashkenas, Irving L., Roger H. Hoh, and Samuel J. Craig, Recommended Revisions to Selected Portions of MIL-F-8785B(ASG) and Background Data, AFFDL-TR-73-76, Nov. 1972.

12. Craig, S. J., and I. L. Ashkenas, Background Data and Recommended Revisions for MIL-F-8785B(ASG), "Military Specification — Flying Qualities of Piloted Airplanes", Systems Technology, Inc., Tech. Rept. 189-1, June 1970.

13. Harlan, Raymond B., and Stephen J. Madden, Jr., A Hazard Definition for Wake Turbulence Encounter During Terminal Area Operations, MIT, Measurement Systems Laboratory, Rept. MIT-MSL-RE-81, 30 Mar. 1973.

APPENDIX A

EMPIRICAL FIT TO B-727 TOWER DATA

The purpose of this appendix is to describe a simple means for fitting vortex flow data with a commonly used analytical expression and then working an example. The analytical expression used to define the tangential flow of a vortex is given in Eq. A-1.

$$V_\theta = \frac{\Gamma_0}{2\pi r}\left[1 - e^{(-r^2/4\epsilon\tau)}\right] \tag{A-1}$$

To simplify the notation during subsequent mathematical manipulations, the following definitions will be used.

$$K \equiv \frac{\Gamma_0}{2\pi} \tag{A-2}$$

$$T \equiv 4\epsilon\tau \tag{A-3}$$

With these definitions Eq. A-1 becomes:

$$V_\theta = \frac{K}{r}\left[1 - e^{(-r^2/T)}\right] \tag{A-4}$$

The goal of the derivation that follows is to determine explicit expressions for K and T in terms of easily measured quantities from wind tunnel or flight tests. Figure A-1 shows a sketch of tangential flow velocity as a function of distance from a vortex center, and defines two quantitites that can be determined from vortex flow measurements (i.e., $V_{\theta_{max}}$ and d_{CORE}). (A second derivation will be presented later where it will be assumed that d_{CORE} is not known.) Thus, the problem at this point is to derive expressions for K and T in terms of $V_{\theta_{max}}$ and d_{CORE}. This is done as follows.

$V_{\theta_{max}}$ is the value of V_θ when

$$\frac{dV_\theta}{dr} = 0 \tag{A-5}$$

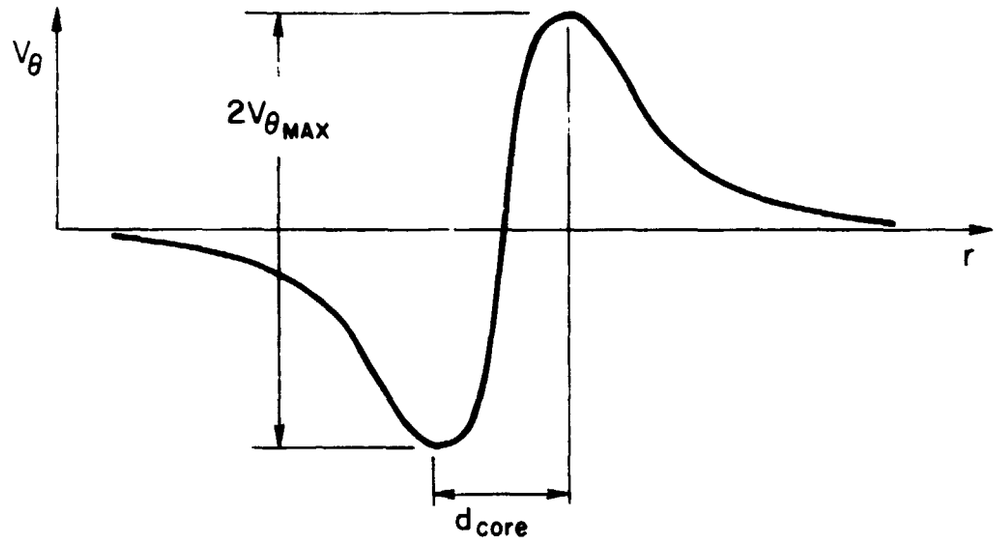

Figure A-1. Sketch of Tangential Flow Velocity for a Single Vortex

Taking a derivative of Eq. A-4 gives,

$$\frac{dV_\theta}{dr} = \frac{-K}{r^2}\left[1 - e^{(-r^2/T)}\right] + \frac{K}{r}\left[\frac{2r}{T}\, e^{(-r^2/T)}\right] \qquad \text{(A-6)}$$

Then, equating this to zero and rearranging terms leads to Eq. A-7.

$$\frac{1}{2}\left[e^{(r_{CORE}^2/T)} - 1\right] = \frac{r_{CORE}^2}{T} \qquad \text{(A-7)}$$

This equation is seen to be a transcendental equation in the single variable, r_{CORE}^2/T. Separate plots of the left and right sides of this equation are shown in Fig. A-2, where it can be seen that two distinct solutions exist: one trivial solution at $r_{CORE}^2/T = 0$, and the desired solution at $r_{CORE}^2/T = 1.25643$. The desired solution can be rewritten in terms of the vortex core diameter (instead of core radius) as,

$$T = \frac{r_{CORE}^2}{1.25643} = \frac{(d_{CORE}/2)^2}{1.25643} \qquad \text{(A-8)}$$

or,

$$T = 0.198976\, d_{CORE}^2 \qquad \text{(A-9)}$$

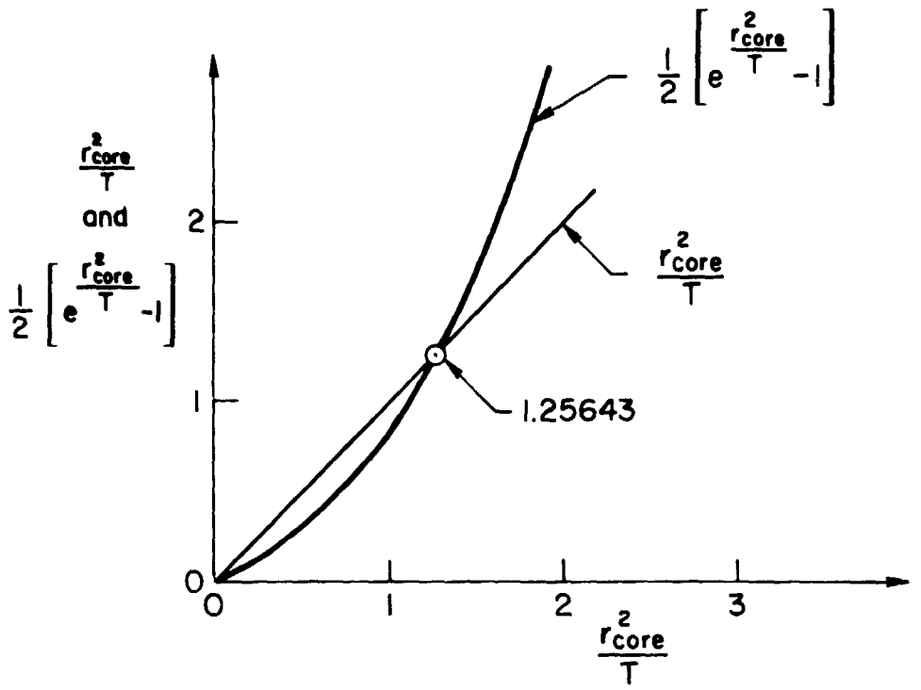

Figure A-2. Plots of Left and Right Sides of Equation A-7

This gives an explicit expression for T in terms of d_{CORE}.

Next we need to derive an expression for K. Substituting the solution for r^2_{CORE}/T into Eq. A-4 and rearranging terms gives,

$$K = 1.39795\ V_{\theta_{max}} r_{CORE} \tag{A-10}$$

or,

$$K = 0.698977\ V_{\theta_{max}} d_{CORE} \tag{A-11}$$

In terms of the total circulation this becomes,

$$\Gamma_o \equiv 2\pi K = 4.39180\ V_{\theta_{max}} d_{CORE} \tag{A-12}$$

Thus, we have determined simple analytical expressions for computing the values of vortex strength (Γ_o) and effective age ($T \equiv 4\varepsilon\tau$) in terms of peak tangential velocity and radius (or diameter) at which this peak velocity occurs. The pertinent equations are repeated here in simplified form for easy reference.

$$\frac{\Gamma_o}{2\pi} = 0.70\, V_{\theta_{max}} d_{CORE} \qquad \text{(A-13)}$$

$$4\varepsilon\tau = 0.20\, d_{CORE}^2 \qquad \text{(A-14)}$$

The above derivation assumes d_{CORE} is known. Many times this is not the case. For those cases where d_{CORE} is not known the following derivation would apply. (Actually, the results that follow can also be applied when d_{CORE} is known, thereby providing a check of the computed estimate of d_{CORE}.)

If Eqs. A-13 and A-14 are substituted into Eq. A-1 (and r_{CORE} is used instead of d_{CORE}), the following equation results.

$$\frac{V_\theta}{V_{\theta_{max}}} = \frac{1.4}{(r/r_{CORE})}\left[1 - e^{-1.25(r/r_{CORE})^2}\right] \qquad \text{(A-15)}$$

For r/r_{CORE} greater than 2 the exponential terms is less than 0.01 and can be neglected, giving,

$$\left.\frac{V_\theta}{V_{\theta_{max}}}\right|_{\frac{r}{r_{CORE}} > 2} = \frac{1.4}{(r/r_{CORE})} \qquad \text{(A-16)}$$

This shows that outside the <u>immediate</u> region of the core the details of core size, etc. have no effect on the flow field.

Such a result suggests that the <u>best</u> way to estimate Γ_o would be to fit the measured flow outside the core region with a curve of the form of Eq. A-17.

$$V_\theta = \frac{\Gamma_o}{2\pi r} \qquad \text{(A-17)}$$

Then Eq. A-13 could be used to estimate d_{CORE} (assuming $V_{\theta_{max}}$ is known); and Eq. A-14 to determine $4\varepsilon\tau$. This progression of calculations avoids the sometimes inaccurate estimate of d_{CORE} obtained through direct measurement.

The following steps summarize the sequence of calculations used when d_{CORE} is either not known, or will only be used for checking the computed value.

- Fit flow data outside of core vicinity with curve of form:

$$V_\theta = \frac{K}{r} \equiv \frac{\Gamma_o}{2\pi r} \tag{A-18}$$

- Use value obtained for $\Gamma_o/2\pi$ along with measured value of $V_{\theta_{max}}$ to compute d_{CORE} via:

$$d_{CORE} = \frac{\Gamma_o/2\pi}{0.70\ V_{\theta_{max}}} \tag{A-19}$$

- Compute $T \equiv 4\epsilon\tau$ (using Eq. A-14):

$$4\epsilon\tau = 0.20\ d_{CORE}^2$$

An example application of this technique for fitting vortex flow data with an analytical expression is given here to demonstrate its usefulness. Figure A-3 shows how the flow outside the core region can be fit with a simple K/r curve. The value of K ($\equiv \Gamma_o/2\pi$) was found to be 250. ft^2/sec for this example data for a B-727. d_{CORE} is now computed to be:

$$d_{CORE} = \frac{\Gamma_o/2\pi}{0.70\ V_{\theta_{max}}} = \frac{250.}{0.7(209.)} = 1.71\ ft \tag{A-20}$$

and $T \equiv 4\epsilon\tau$ is found as:

$$T \equiv 4\epsilon\tau = 0.20\ d_{CORE}^2 = 0.58\ ft^2 \tag{A-21}$$

With these numerical values Eq. A-1 becomes,

$$V_\theta = \frac{250.}{r}\left[1 - e^{(-r^2/0.58)}\right] \tag{A-22}$$

A plot of this equation along with the superimposed data points is shown in Fig. A-4.

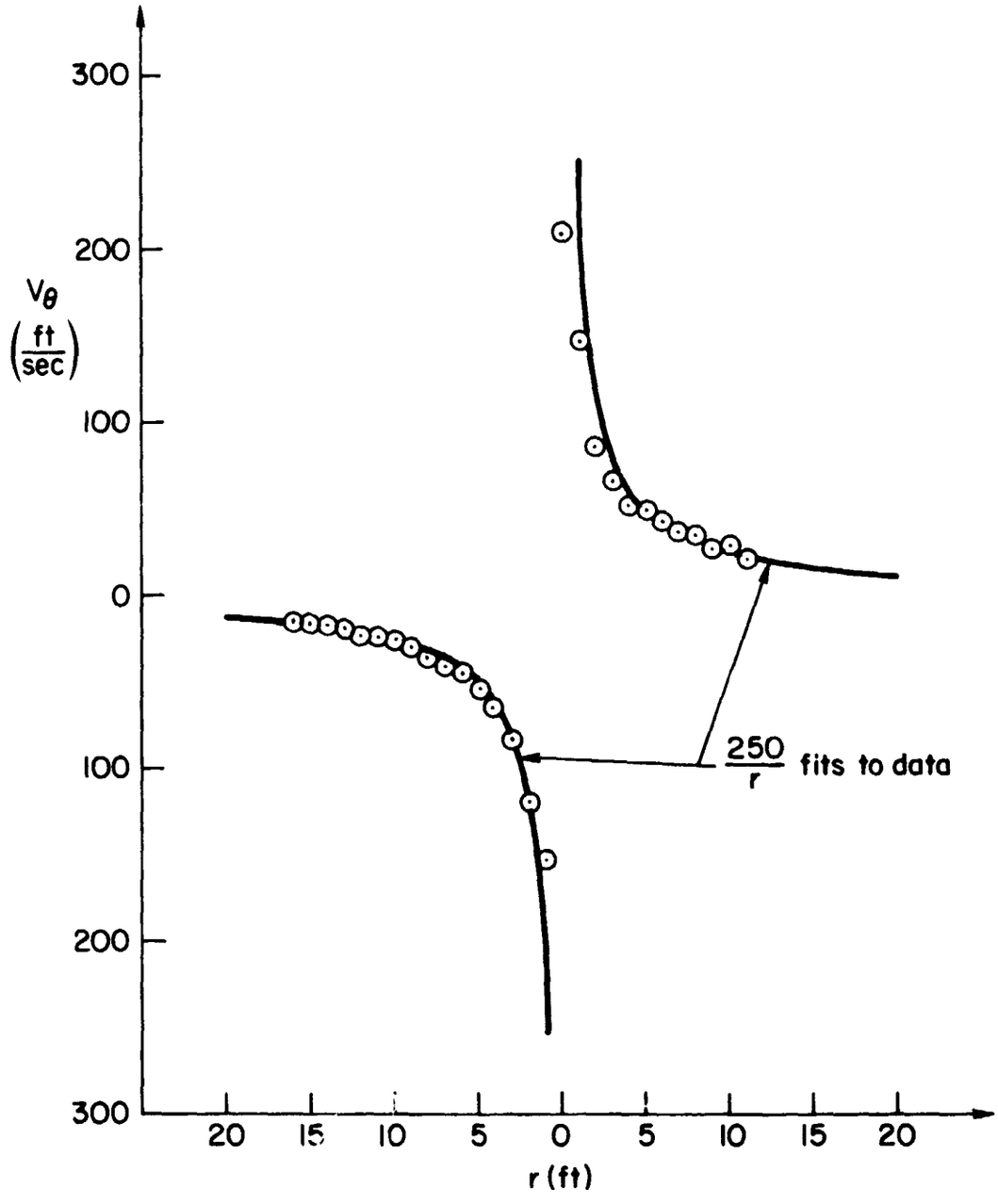

Figure A-3. K/r Fit to Vortex Flow Data for a B-727

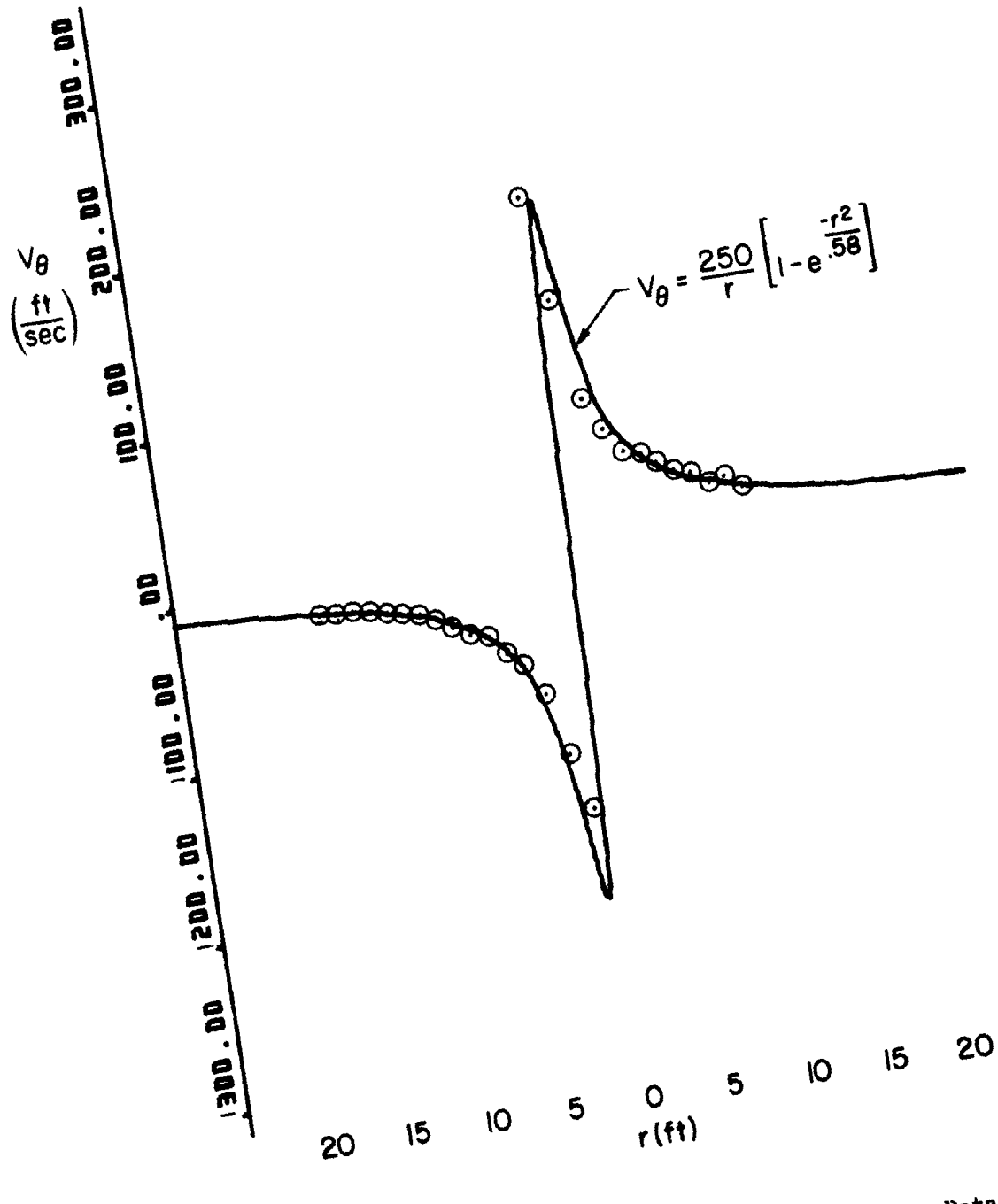

Figure A-4. Analytical Fit of B-727 Vortex Flow Data

APPENDIX B

DERIVATION OF VORTEX FLOW AND STRIP THEORY EQUATIONS

VORTEX MODEL

The vortex model used, which was taken from Ref. 1, is defined by the tangential flow characteristics given below (because no good model for axial flow is known, it was set equal to zero, thus giving a two-dimensional flow).

$$V_T = \frac{\Gamma_o}{2\pi r}\left[1 - e^{-\left(\frac{r^2}{4\epsilon\tau}\right)}\right] \qquad \text{(B-1)}$$

where

V_T is the tangential vortex velocity

Γ_o = $4W_G/\pi\rho V_G b_G$ represents the strength of the vortex (it is a function of the weight, speed, and wing span of the generating airplane)

ϵ = $0.0002\ \Gamma_o$ represents the vortex decay effect

τ represents the age of the vortex

r is the radial distance from the center of the vortex

The centers of the two vortices from the generating airplane are assumed to be straight lines at a constant altitude, parallel to each other at a distance $(\pi/4)b_G$ apart (Ref. 1). A sketch of the resulting vertical flow from both vortices is shown in Fig. B-1.

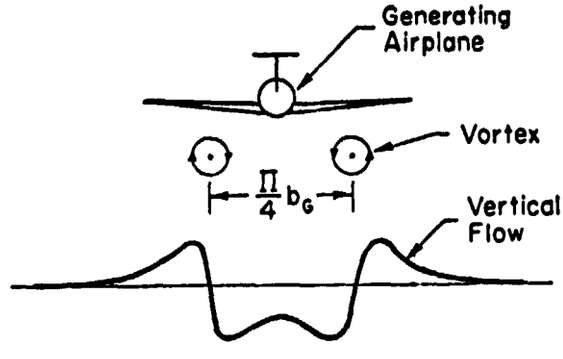

Figure B-1. Sketch of the Vortex Flow Field

STRIP THEORY

Because the vortices produce a highly nonuniform local flow over the lifting surfaces of the penetrating airplane, strip theory was used to compute the forces and moments caused by the vortex flow (see Ref. 5). To implement this, the penetrating airplane was assumed to have three lifting surfaces: a wing, a horizontal tail, and a vertical tail. Each of these surfaces was divided into chord-wise strips as shown in Fig. B-2. The wing was divided into 20 strips per semi-span, while the horizontal and vertical tails were each divided into 6 strips per semi-span. The distributed forces along the fuselage were modeled via a pitching moment and a yawing moment respectively proportional to the vortex-flow-induced incremental angles of attack and sideslip measured at the wing 1/4 root chord.

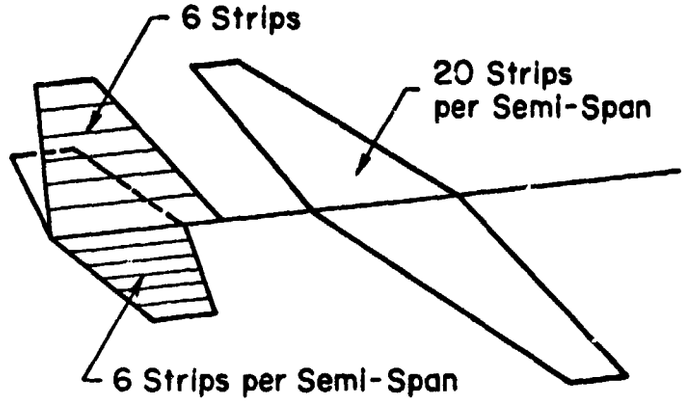

Figure B-2. Strip Theory Geometry

FLOW AT EACH STRIP

Let $\bar{w}_{i_E}$ be the velocity vector of the wind at any point (i) in space (due to both vortices) expressed in "earth-fixed" axes.

$$\bar{w}_{i_E} \equiv \begin{pmatrix} w_x \\ w_y \\ w_z \end{pmatrix}_E \qquad \text{(B-2)}$$

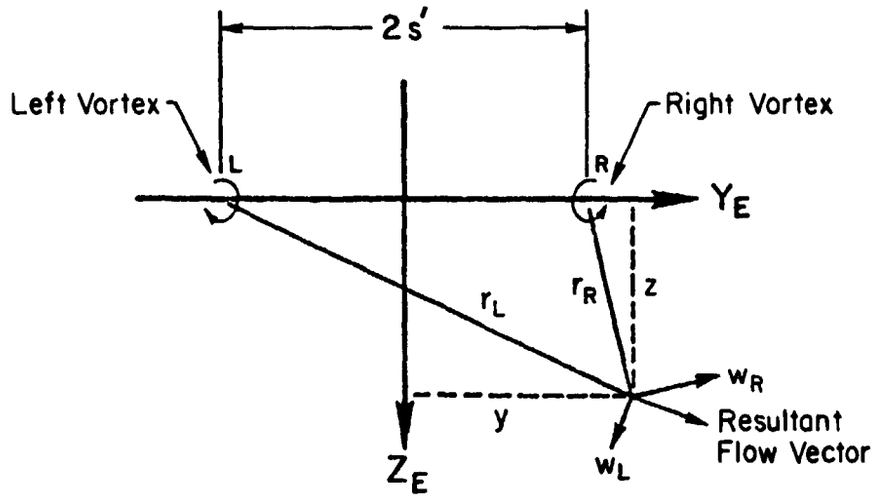

Figure B-3. Flow at an Arbitrary Point in Space (y , z) Due to the Left and Right Vortices of a Generating Airplane

From Fig. B-3 it can be seen that:

$$w_x = 0 \tag{B-3}$$

$$w_y = -w_L\left(\frac{z}{r_L}\right) + w_R\left(\frac{z}{r_R}\right) \tag{B-4}$$

$$w_z = +w_L\left(\frac{y + s'}{r_L}\right) - w_R\left(\frac{y - s'}{r_R}\right) \tag{B-5}$$

where w_L and w_R are the tangential flow magnitudes of the left and right vortices, respectively.

Clearly, $\bar{w}_{i_E}$ is a function of the position of the point in space being considered ($\bar{R}_{i_E}$); i.e., $\bar{w}_{i_E} = \bar{w}_{i_E}(\bar{R}_{i_E})$. But points of interest for flow calculations will be points on the airplane expressed in airplane body axes. Thus:

$$\bar{R}_{i_E} = \bar{R}_{cg_E} + T\,\bar{R}_{i_B} \tag{B-6}$$

where

$\bar{R}_{cg_E}$ is the position of the airplane c.g. in earth axes

T is the transformation matrix from airplane body axes to earth axes

$\bar{R}_{i_B}$ is the position of a point on the airplane expressed in airplane body axes

$$\bar{R}_{cg_E} = \begin{pmatrix} x_{cg} \\ y_{cg} \\ z_{cg} \end{pmatrix}_E \tag{B-7}$$

$$\bar{R}_{i_B} = \begin{pmatrix} x_i \\ y_i \\ z_i \end{pmatrix}_B \tag{B-8}$$

$$T = \begin{bmatrix} \cos\psi\cos\theta & \cos\psi\sin\theta\sin\varphi - \sin\psi\cos\varphi & \cos\psi\sin\theta\cos\varphi + \sin\psi\sin\varphi \\ \sin\psi\cos\theta & \sin\psi\sin\theta\sin\varphi + \cos\psi\cos\varphi & \sin\psi\sin\theta\cos\varphi - \cos\psi\sin\varphi \\ -\sin\theta & \cos\theta\sin\varphi & \cos\theta\cos\varphi \end{bmatrix} \tag{B-9}$$

For force calculations we need to know the flow (due to the vortices) in airplane body axes. Thus:

$$\bar{w}_{i_B} = T^{-1}\,\bar{w}_{i_E} \tag{B-10}$$

Note that:

$$\bar{w}_{i_B} = \begin{pmatrix} u_i \\ v_i \\ w_i \end{pmatrix}_B \tag{B-11}$$

The incremental angles of attack and sideslip are defined as:

$$\Delta\alpha_i \equiv \frac{-w_i}{V} \tag{B-12}$$

$$\Delta\beta_i \equiv \frac{-v_i}{V} \tag{B-13}$$

Putting all this together gives:

$$\begin{pmatrix} 0 \\ \Delta\beta_i \\ \Delta\alpha_i \end{pmatrix}_B = \frac{-1}{V} [T]^{-1} \begin{pmatrix} 0 \\ w_y \\ w_z \end{pmatrix}_E \tag{B-14}$$

or,

$$\begin{pmatrix} 0 \\ \Delta\beta_i \\ \Delta\alpha_i \end{pmatrix}_B = \frac{-\Gamma_o}{2\pi V} [T]^{-1} \begin{bmatrix} 0 \\ \left[\frac{-z}{z^2+(y+s')^2}\right]\left[1 - e^{\frac{-z^2-(y+s')^2}{4\epsilon\tau}}\right] + \left[\frac{z}{z^2+(y-s')^2}\right]\left[1 - e^{\frac{-z^2-(y-s')^2}{4\epsilon\tau}}\right] \\ \left[\frac{y+s'}{z^2+(y+s')^2}\right]\left[1 - e^{\frac{-z^2-(y+s')^2}{4\epsilon\tau}}\right] - \left[\frac{y-s'}{z^2+(y-s')^2}\right]\left[1 - e^{\frac{-z^2-(y-s')^2}{4\epsilon\tau}}\right] \end{bmatrix}_E \tag{B-15}$$

and

$$\begin{pmatrix} x \\ y \\ z \end{pmatrix}_E = \begin{pmatrix} x_{cg} \\ y_{cg} \\ z_{cg} \end{pmatrix}_E + [T] \begin{pmatrix} x_i \\ y_i \\ z_i \end{pmatrix}_B \tag{B-16}$$

The components x_i, y_i, z_i (in body axes) will be given in the next subsection.

AIRPLANE GEOMETRY AND INCREMENTAL FORCES INDUCED ON EACH STRIP

The incremental force on each strip is assumed to act at the intersection of the 0.25 $\bar{c}$ and the centerline of the strip and is proportional to the incremental angle of attack at the 0.75 $\bar{c}$ of the strip (Ref. 5). The geometry required to define the pertinent locations on the lifting surfaces is given in Fig. B-4; and the resulting equations follow. The subscript "i" is used for the right side of the airplane and for the vertical tail, while "j" is used for the left side of the airplane. i and j both increase from root to tip.

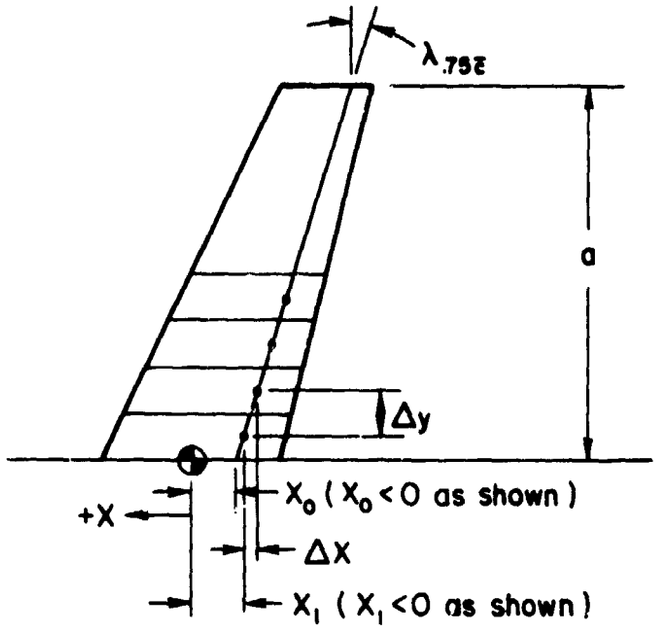

N ≡ Number of Strips Per Side

$\Delta y = \frac{a}{N}$

Figure B-4. Geometry for Typical Lifting Surface (Note that Similar Relations Apply to 0.25 $\bar{c}$ and 0.75 $\bar{c}$ Locations)

Wing and Horizontal Tail:

$$X_{i+1} = X_i - \Delta x = X_i - \Delta y \tan \lambda$$

$$X_{\substack{i+1 \\ j+1}} = X_{\substack{i \\ j}} - \frac{a}{N} \tan \lambda \qquad \text{(B-17)}$$

$$X_1 = X_o - \frac{a}{2N} \tan \lambda \qquad \text{(B-18)}$$

$$y_{i+1} = y_i + \frac{a}{N} \qquad \text{(B-19)}$$

$$y_{i=1} = \frac{a}{2N} \qquad \text{(B-20)}$$

$$y_{j+1} = y_j - \frac{a}{N} \qquad \text{(B-21)}$$

$$y_{j=1} = -\frac{a}{2N} \qquad \text{(B-22)}$$

$$z_{\substack{i \\ j}} = \text{constant (for wing and horizontal tail)} \qquad \text{(B-23)}$$

Vertical Tail:

$$X_{i+1} = X_i - \frac{a}{N} \tan \lambda \qquad \text{(B-24)}$$

$$X_1 = X_o - \frac{a}{2N} \tan \lambda \qquad \text{(B-25)}$$

$$y_i = 0 \qquad \text{(B-26)}$$

$$Z_{i+1} = Z_i - \frac{a}{N} \qquad \text{(B-27)}$$

$$Z_1 = Z_o - \frac{a}{2N} \qquad \text{(B-28)}$$

AREAS OF STRIPS

Figure B-5 and the following two equations define the area of each strip.

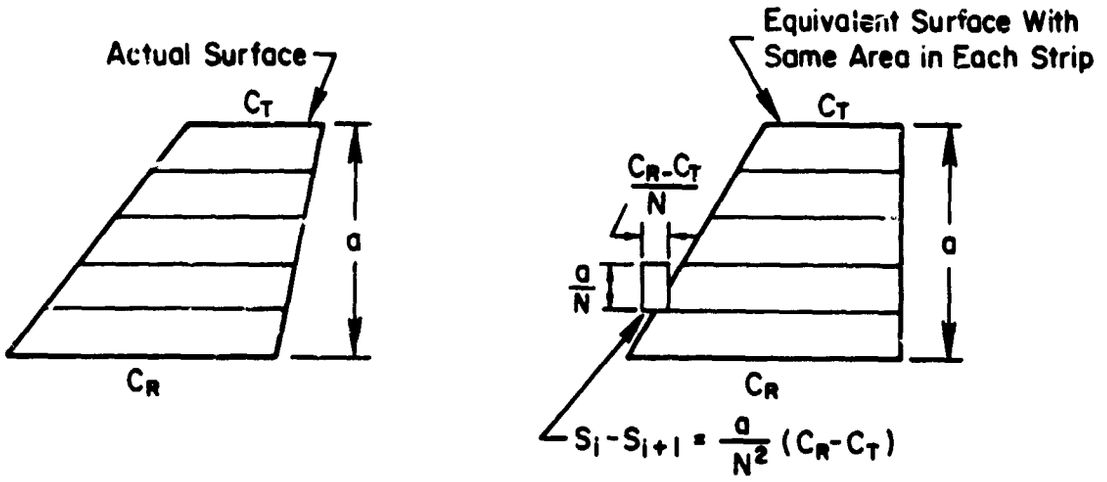

Figure B-5. Geometry Pertinent to Determining Area of Each Strip

$$S_{i+1} = S_i - \frac{a}{N^2}(C_R - C_T) \qquad \text{(B-29)}$$

$$S_1 = \frac{a}{N}\left[C_R - \frac{1}{2N}(C_R - C_T)\right] \qquad \text{(B-30)}$$

INCREMENTAL FORCES

The incremental forces on each strip are summed as shown below to give the net forces and moments on the airplane. ΔX_{vortex} is ignored. The notation used here is defined as follows.

W ≡ Wing

H ≡ Horizontal tail

V ≡ Vertical tail

F ≡ Fuselage

$$\Delta Z_{vortex} = -\bar{q}\left[C_{L_{\alpha_W}}\left(\sum_{i=1}^{N_W} S_{W_i}\alpha_{W_i} + \sum_{j=1}^{N_W} S_{W_j}\alpha_{W_j}\right)\right.$$

$$\left. + C_{L_{\alpha_H}}\left(1 - \frac{d\epsilon}{d\alpha}\right)\left(\sum_{i=1}^{N_H} S_{H_i}\alpha_{H_i} + \sum_{j=1}^{N_H} S_{H_j}\alpha_{H_j}\right)\right] \qquad (B\text{-}31)$$

$$\Delta Y_{vortex} = -\bar{q}C_{L_{\alpha_V}}\left(1 - \frac{d\sigma}{d\beta}\right)\sum_{i=1}^{N_V} S_{V_i}\beta_{V_i} \qquad (B\text{-}32)$$

$$\Delta L_{vortex} = \bar{q}\left[-C_{L_{\alpha_W}}\left(\sum_{i=1}^{N_W} S_{W_i}\alpha_{W_i}y_{W_i} + \sum_{j=1}^{N_W} S_{W_j}\alpha_{W_j}y_{W_j}\right)\right.$$

$$-C_{L_{\alpha_H}}\left(1 - \frac{d\epsilon}{d\alpha}\right)\left(\sum_{i=1}^{N_H} S_{H_i}\alpha_{H_i}y_{H_i} + \sum_{j=1}^{N_H} S_{H_j}\alpha_{H_j}y_{H_j}\right)$$

$$\left. + C_{L_{\alpha_V}}\left(1 - \frac{d\sigma}{d\beta}\right)\sum_{i=1}^{N_V} S_{V_i}\beta_{V_i}z_{V_i}\right] \qquad (B\text{-}33)$$

$$\Delta M_{vortex} = \bar{q}\left[C_{L_{\alpha_W}}\left(\sum_{i=1}^{N_W} S_{W_i}\alpha_{W_i}x_{W_i} + \sum_{j=1}^{N_W} S_{W_j}\alpha_{W_j}x_{W_j}\right) + M_{\alpha_F}\alpha_F\right.$$

$$\left. + C_{L_{\alpha_H}}\left(1 - \frac{d\epsilon}{d\alpha}\right)\left(\sum_{i=1}^{N_H} S_{H_i}\alpha_{H_i}x_{H_i} + \sum_{j=1}^{N_H} S_{H_j}\alpha_{H_j}x_{H_j}\right)\right] \qquad \text{(B-34)}$$

$$\Delta N_{vortex} = \bar{q}\left[-C_{L_{\alpha_V}}\left(1 - \frac{d\sigma}{d\beta}\right)\sum_{i=1}^{N_V} S_{V_i}\beta_{V_i}x_{V_i} + N_{\beta_F}\beta_F\right] \qquad \text{(B-35)}$$

α_F and β_F are evaluated at the 0.25 $\bar{c}$ of the wing root chord.

It is noted that stall was accounted for by limiting the maximum (and minimum) lift coefficient on each strip.

APPENDIX C

HANDLING QUALITIES CONSIDERATIONS

The PA-30 bank angle command systems presented in Section VI were based on optimizing the response to vortex upsets. The purpose of this appendix is to determine if the initial control system (with the high roll rate gain) plus airplane results in adequate handling properties for normal operations. To be consistent with the vortex analysis, the handling qualities evaluation assumes the aircraft to be in the landing configuration at 100 kt (full flaps, gear down).

A summary of pertinent lateral handling quality factors are given in Table C-1 where each of the handling metrics for the augmented airplane are compared to the bare airplane and to "desirable values" as determined from Refs. 10, 11, and 12.

The dutch roll frequency and damping of the augmented airplane are seen to be well above the minimum requirements (see Table C-1). A significant improvement in dutch roll damping is evident on the augmented airplane as compared to the bare airplane. While the bare airplane is seen to be quite acceptable in this regard, the combination of minimal dutch roll damping ($\zeta_d = 0.225$) and low $|\phi/\beta|_{d.r.}$ usually results in an uncomfortable "snaking motion" in turbulence. It is therefore expected that the pilot ratings in turbulence will improve from acceptable (order of 3) to very good (order of 1.5) as a result of the augmentation.

The roll subsidence and spiral modes for the bare airplane are also well within acceptable limits (see Table C-1). However, for many augmented airplanes (including this one) the roll subsidence and spiral modes do not exist in the conventional sense. In the present case, the roll rate to aileron feedback results in a coupling between the roll mode pole and the actuator mode pole giving a second-order mode at a frequency of 13 rad/sec and a damping ratio of 0.5. The bank angle to aileron feedback stabilizes the unstable spiral mode and drives the spiral mode pole out to 0.62. The "roll mode" listed at 12 rad/sec in Table C-1 actually only represents the time required to achieve peak roll rate for a step aileron input.

TABLE C-1

HANDLING QUALITY PARAMETERS

	DESIRABLE VALUES	AUGMENTED PA-30	BARE PA-30
ω_d	> 1.0 (rad/sec)	2.7 (rad/sec)	2.57 (rad/sec)
ζ_d	> 0.08	0.708	0.225
$\zeta_d\omega_d$	> 0.15 (rad/sec)	1.91 (rad/sec)	0.58 (rad/sec)
$1/T_R$	1.0 (1/sec)	12.0 (1/sec)	4.167 (1/sec)
$1/T_s$	>-0.034 (1/sec)	0.62 (1/sec)	-0.0164 (1/sec)
ω_φ/ω_d	0.75-1.1	0.96	0.85
P_{max}	>10.0 (deg/sec)	33. (deg/sec)	35. (deg/sec)
$\left\|\frac{\varphi}{\beta}\right\|_{d.r.}$	< 1.5	0.16	0.83
μ	See Fig. C-1	-0.24	0
$\left(\frac{N'_{\delta_w}}{L'_{\delta_w}}\right)$	See Fig. C-1	-0.17	-0.20
$\varphi_{t=1.3\ sec}$	≥ 30 (deg)	37 (deg)	40 (deg)

The bank angle attainable in 1.3 sec for a full lateral wheel input is given as a measure of adequate control authority in Ref. 10. From Table C-1 it is seen that the unaugmented and augmented configurations both have adequate control power.

Having established that the inner-loop (bank angle) characteristics are satisfactory, the outer (heading) loop characteristics may be identified. Evaluation of the piloted heading control properties is accomplished via the aileron-rudder coordination boundaries taken from Ref. 11 and given in Fig. C-1. The μ parameter (ordinate in Fig. C-1) defines the rudder shaping required to coordinate the turn and the $N'_{\delta_w}/L'_{\delta_w}$ (abscissa in Fig. C-1) parameter defines the required magnitude. From Table C-1, the values of μ for the augmented and unaugmented airplanes are small

($|u| << 1$), indicating a pure gain rudder is required (see Ref. 11). In both cases, the rudder magnitude is well within the 3.5 pilot rating boundary. We therefore would expect favorable pilot ratings for heading control for the augmented as well as the unaugmented airplane. It is interesting to note that the yaw damper is somewhat unconventional in that the yaw rate feedback is not washed out. Classical SAS "design rules" require a washout on the yaw rate feedback to avoid the effect of "opposite rudder" in a steady turn. However, the pilot rating boundaries in Fig. C-1 indicate that the pilot will supply the required rudder without degradation in opinion rating. Based on these results, we conclude that the simplified yaw damper CAS (no washout) will have little (if any) effect on pilot opinion.

In summary, the initial (high roll rate gain) PA-30 stability augmentation system design based on minimizing the response to wake vortex encounters is expected to result in favorable pilot opinion for normal flight operations.

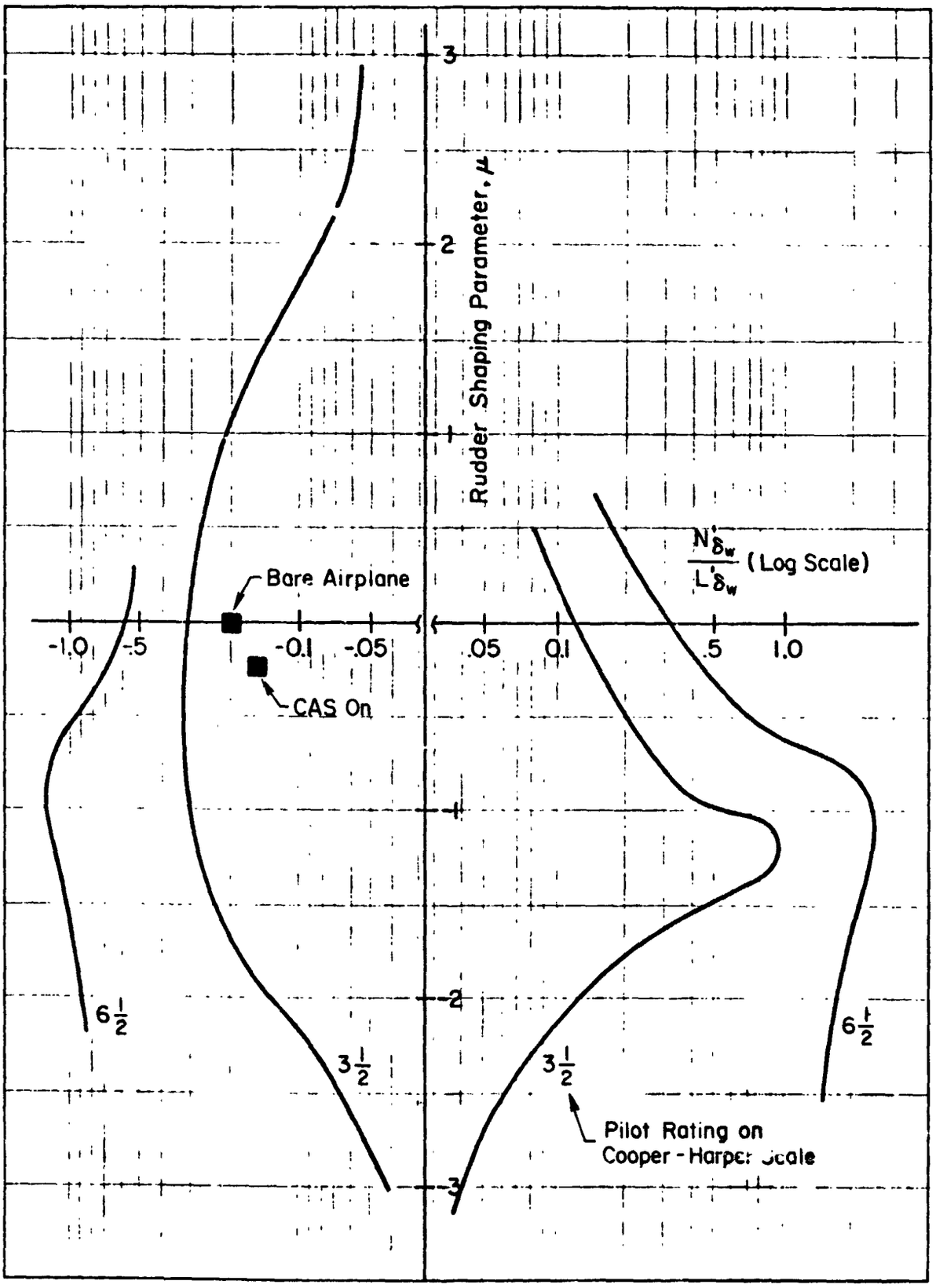

Figure C-1. Pilot Rating Boundaries for Heading Control

APPENDIX D

FLIGHT TEST ACTIVITIES

A limited flight test program was carried out at NASA's Flight Research Center in early November of 1973 to investigate vortex characteristics and encounter upsets. A Boeing 727 was used as the generating aircraft (to generate vortices), and a PA-30 and a Learjet were used as penetrating aircraft. The primary tests were carried out at an altitude of 12,000 ft to insure adequate altitude for upset recovery as well as to avoid convective turbulence present near the ground (which would tend to break up the vortices).

The PA-30 was fully instrumented to record airplane motions during vortex encounters. While the Learjet was also instrumented to measure airplane motions, in addition it was equipped with flow measuring apparatus and was thus used primarily to measure the vortex flow at separations (from the generator) near those of the PA-30 penetrations.

All of the vortex penetrations were essentially axial. The attempts to obtain flow data via perpendicular crosstrack encounters with the Learjet were only moderately successful, because the smoke used to visualize the vortices was not dense enough to be seen from the side (except at very close ranges).

The digital simulation was utilized to investigate several aspects of the proposed vortex encounters prior to the flight tests. These were to determine if there might be a potential safety nazard as regards structural loads on the lifting surfaces, as well as to give the pilot an indication of the severity of the upsets to expect. With regard to the load calculations, a significant aspect remains unresolved. This is how to account for the dynamic lift effect due to the very rapid buildup of angle of attack during the penetration of a vortex core. As an approximation for the load calculations it was assumed that the maximum lift coefficient on a strip is 1.25 times the value for static stall.

One of the hoped for results of the flight tests was a validation of the assumed human pilot model (at least for the "expectant" pilot situation). However, there was considerable difficulty in getting <u>any</u> quantitative results

with the available flight test data. In fact, due to the large uncertainties in the data no direct model validation was even attempted. Therefore, we were able to make only a few qualitative statements concerning the pilot's control actions. One of these is that the pilot appears to be applying aileron proportional to bank angle (with a gain of about unity) prior to the large vortex induced upsets. Then he appears to approximately double his aileron gain when a large rolling disturbance occurs. It is noted that the gain levels measured are consistent with what would be predicted analytically, but the small amount of good flight data does not justify making any general conclusions. To get some feel for the type of control activity used, Figure D-1 shows examples of bank angle and aileron traces during two vortex encounters.

We would also like to have obtained some "surprised" pilot data wherein the pilot was not mentally prepared for the vortex encounter, but there were no instances of this situation during the flight tests. Therefore, a pilot model for such a situation is pure speculation at this point.

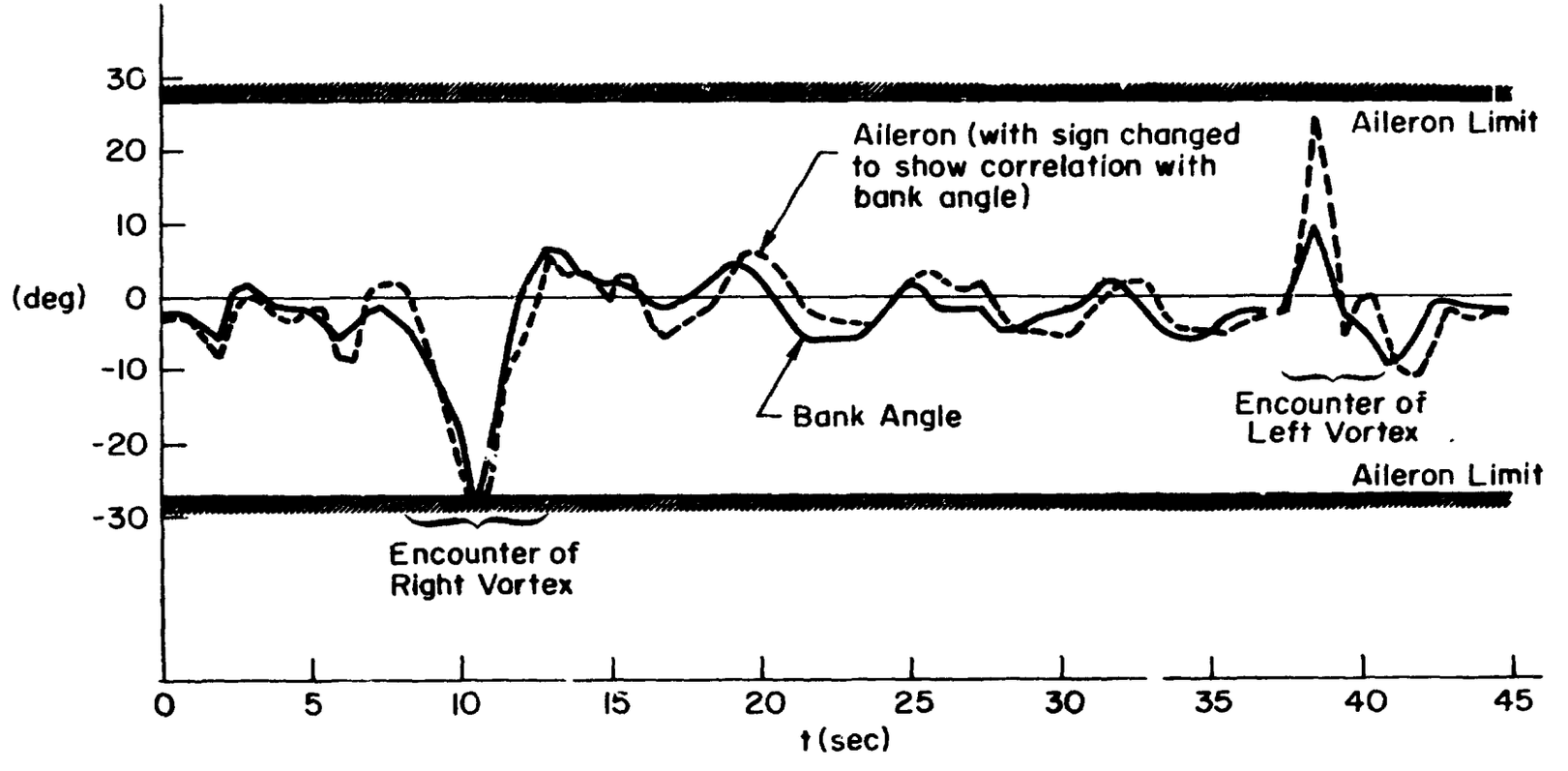

Figure D-1. Flight Test Bank Angle and Aileron Time Traces Showing Axial Encounters of Both Left and Right Vortices